DESIGN AND FABRICATION OF A PARABOLIC DISH SOLAR COLLECTOR WITH A THERMAL COMPENSATOR

MUHIA NGARUIYA

MASTER OF SCIENCE

(Physics)

JOMO KENYATTA UNIVERSITY OF

AGRICULTURE AND TECHNOLOGY

2016

Design and Fabrication of a Parabolic Dish Solar Collector with a Thermal Compensator

Muhia Ngaruiya

A Thesis Submitted in Fulfillment for the Degree of Master of Science in Physics in the Jomo Kenyatta University of Agriculture and Technology.

2016

DECLARATION

This thesis is my original work and has not been presented elsewhere for a degree award.

Signature…….Date……

Muhia Ngaruiya

This thesis has been submitted for examination with our approval as university supervisors.

Signature…….. Date…….

Prof. Robert Kinyua, (PhD)

JKUAT, Kenya

Signature…….. Date…….

Dr. Joseph Ngugi Kamau, (PhD)

JKUAT, Kenya

DEDICATION

This work is dedicated to my wife Sarah Wanjiku and children Margaret Nyokabi and Paul Moiya. That the effort, time and resources put in this cause is not in vain.

ACKNOWLEDGEMENTS

I wish to acknowledge the support and guidance of my very resourceful supervisors: Prof. Kinyua and Dr. Kamau who have encouraged me to go on even in times of financial challenges when doing this unfunded project. Mr. Wahinya of engineering workshop, who tirelessly helped me in welding work and all the workshop staff for their cooperation. My acknowledgements also go to my wife Sarah Wanjiku who gave me moral support and endured constrained budget during my study.

TABLE OF CONTENTS

LIST OF TABLES

LIST OF FIGURES

LIST OF PLATES

ABBREVIATIONS AND ACRONYMS

AM	Air Mass
EMW	Electromagnetic Waves
ERC	Energy Regulatory Commission
HTF	Heat transfer fluid
IR	Infrared Radiation
LHS	Latent heat storage
NEMA	National Environment Management Authority
PCM	Phase Change Material
PDR	Parabolic Dish Reflector
PDSC	Parabolic Dish Solar Concentrator
PVC	Photovoltaic Cell
SED	Solar Energy Devices
SHS	Sensible heat storage
SWERA	Solar and Wind Energy Resources Assessment
UV	Ultra Violet
WRDC	World Radiation Data Center

LIST OF SYMBOLS

η	Efficiency
η_1	First law efficiency
$\dot{m}$	Mass flow rate
T_i	Inlet temperature of water
T_o	Outlet temperature of water
A_a	Dish aperture area
A_r	Receiver/Absorber area
Δt	Time interval
G_{sc}	Solar radiation/Solar constant
Q_s	Stored Thermal energy
C_p	Heat capacity at constant pressure
C	Concentration ratio
C_f	Concentration factor
F	Focus
R	Radius of dish aperture
r	Radius of receiver
λ	Wavelength of electromagnetic waves

γ	Intercept factor
A	Ability to store thermal energy
ρ	Density
r	Reflectance
A_{ae}	Effective aperture area

ABSTRACT

Solar energy is a free natural resource but its harvesting requires a high capital investment which prohibits its maximum exploitation. Moreover, most solar collectors do not give steady energy output due to fluctuating solar radiation caused by intermittent cloud cover. A Parabolic Dish Solar Collector (PDSC) with a thermal storage-recovery system has been developed to harness solar beam radiation and give steady energy output. The system was constructed using steel rods curved to obey the equation of a parabola then welded together with circular support rings. The inside curvature was filled with 3-ply wood to make a parabolic substrate. The substrate was then lined with reflective aluminium foil fitted with adhesive paste. The receiver was made of blackened copper bulb containing tin/lead alloy [60Sn40Pb, melting point = 172^{o}C] engulfing a coiled copper tube carrying water as the heat transfer fluid. The alloy served as a Phase Change Material (PCM) for storing latent heat of fusion. The receiver was positioned at the focus of the parabolic reflector and was supported by a central antenna. The dish was mounted on an axle pivot driven by tension of a spring so as to track the sun along the equatorial latitude. The dish was inclined at an angle of 7.5^{o} which was the solar declination during the season. During cloud cover the thermal storage material would lose sensible heat and latent heat of fusion to the flowing water, thus compensating for the absent solar energy. Efficiency, η of the system was determined by measuring the inlet and outlet temperature of water then calculation done as the ratio of heat gain per unit time against solar power intercepted by the aperture. The maximum efficiency with thermal compensator was 44.82% and minimum efficiency was 3.44% as compared to maximum efficiency of 11.6% and the minimum efficiency of 2.05% without thermal compensator. Thermal compensation factor, C_f was determined by simulating a cloudy condition by temporarily obstructing the dish aperture then measuring the energy output. On a clear day, the system was able to produce steam for various applications. The Solar Energy Device (SED) was found to give fairly stable and reliable energy loading during the solar harvesting period.

CHAPTER ONE

INTRODUCTION AND LITERATURE REVIEW

This chapter contains introduction and literature survey on the solar energy potential, theoretical considerations of reflective type solar thermal concentrators, their setbacks and possible improvements.

1.1 Introduction

The world is headed for a great energy crisis if its overdependence on conventional energy sources continues unchecked (Stefan, Kenneth & Kim, 2006; Global Economic Symposium, 2014). The rapidly growing population of the world is overstretching the finite energy resources while replenishment by biomass cycles and fossilization is not near commensurate with the energy demand. More so the continued use of conventional fuels is greatly degrading the environment through carbon dioxide (CO_2) emission resulting in unsustainable energy balance and accrued economic losses (John, Twidel, & Weir, 1986). Table 1.1 and Fig. 1.1 show a worrying trend in global CO_2 concentration in the atmosphere and atmospheric temperatures indicative of global warming between year 1979 and year 2005. This, if projected to the future may reveal much higher concentrations of CO_2 given the ever expanding industrial activities.

The various forms of energy in use today though manifest in different forms are derived from the sun and comprise of only a small fraction of the infinite solar energy. According to Solar and Wind Energy Resources Assessment (SWERA, 2010), the main application of direct solar energy in most parts of the world especially Africa is drying and space heating. Governments across the world are legislating policies that encourage the use of green energy with a new focus on renewable energy (Energy, 2000), Plate A7. In Kenya, the Energy Regulatory Commission (ERC) is charged with implementing the policy for cost-effective, affordable, adequate and quality energy services (National Energy Policy, 2004). The National Environment Management Authority (NEMA) is

imposing heavy penalties against emitters of green house gases, especially CO_2, in an attempt to discourage the use of fire wood and fossil fuels.

Various Solar Energy Devices (SED) that have been developed, however have not been able to mitigate the challenges because of their high capital investment. In this project, a Parabolic Dish Solar Collector (PDSC) with a thermal compensator has been designed to harness beam radiation from the sun and produce steam for various uses. Made from locally available materials, the cost of construction of PDSC is appreciably reduced and the temporary heat storage fairly stabilizes energy output to match with conventional energy needs.

Table 1.1: Concentrations of CO_2 and global temperature differences for the period 1979- 2005 (WRC Database 2005)

Year		1979	1980	1981	1982	1983	1984	1985	1986
CO_2 (ppm)	concentration	336.53	338.34	339.96	341.09	342.07	344.04	345.10	346.85
ΔT (^oC)		0.06	0.01	0.13	0.12	0.19	-0.01	-0.02	0.02

Year		1987	1988	1989	1990	1991	1992	1993	1994
CO_2 (ppm)	concentration	347.75	350.68	352.84	354.22	355.51	356.39	356.98	358.19
ΔT (^oC)		0.17	0.16	0.1	0.25	0.20	0.06	0.11	0.17

Year		1995	1996	1997	1998	1999	2000	2001	2002
CO_2 (ppm)	concentration	359.82	361.82	362.98	364.90	367.87	369.22	370.44	372.31
ΔT (^oC)		0.27	0.13	0.36	0.52	0.27	0.24	0.40	0.45

Year		2003	2004	2005
CO_2 (ppm)	concentration	374.75	376.95	378.55
ΔT (^oC)		0.45	0.44	0.47

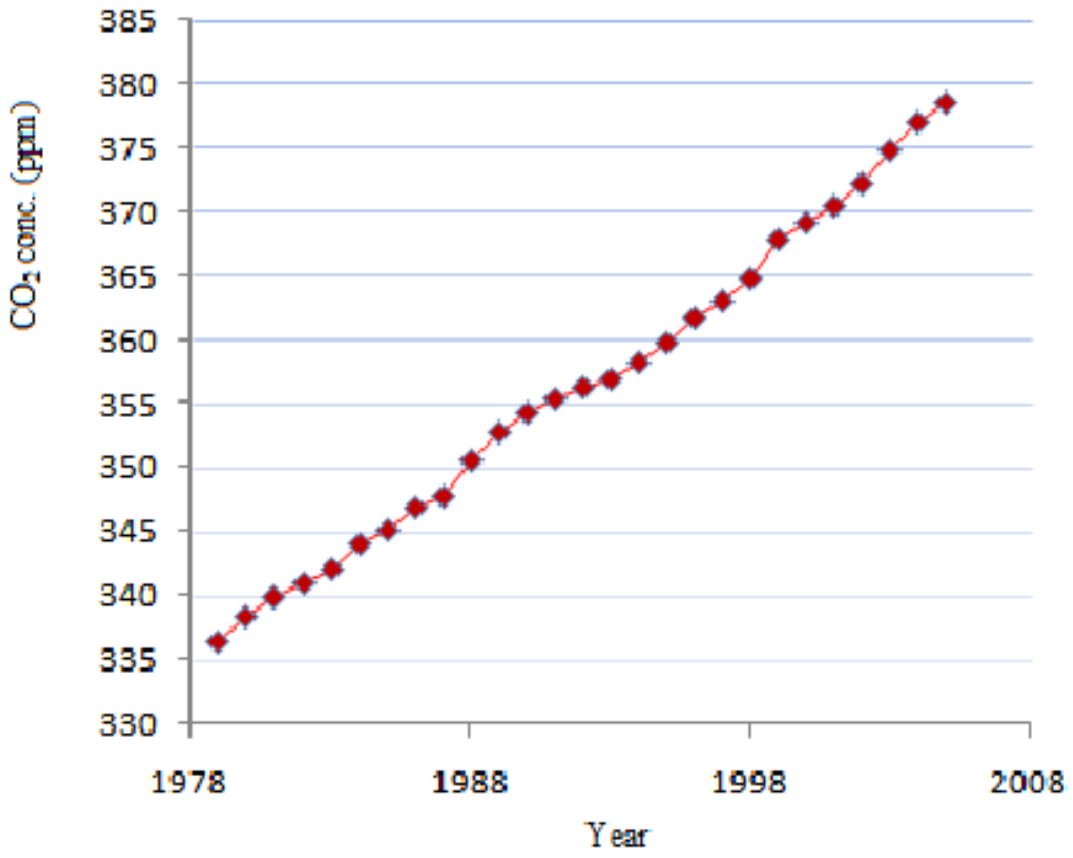

Figure 1.1: Global trend in CO_2 concentration in the atmosphere [WRDC]

1.2 Statement of the problem

Solar energy is the most abundant energy resource yet it is among the most underutilized. The major reason for its underuse is the high capital investment that goes with construction of solar collectors coupled with the fact that the components of solar tracking require external power which is not available in off-grid locations. Furthermore, most solar collectors do not give consistent energy output due to fluctuating solar radiation caused by intermittent cloud cover.

1.3 Justification

Using locally available and recycled materials, the construction cost of the Solar Energy Device could be greatly reduced to affordable levels by poor communities. Moreover, the use of a design that compensates energy output provides reliable energy loading which is compatible with conventional energy needs ((Banaszek, Domanaski, Rebow, & El-Sagier, 1999; Thulasi, Karmakar, & Rao, 1994). In Kenya, which is mapped as a high insolation region by world radiation center, domestic cooking and heating activities occurring during the day can utilize the abundant solar thermal energy. Vast amounts of wood fuel, oil, gas, and electricity that are consumed would be saved annually. The system can significantly reduce the cost of domestic fuels at the same time mitigating CO_2 emission for sustainable environment.

1.4 Objectives

1.4.1 General objective

The general objective of this study is to design and fabricate a parabolic dish solar collector with a thermal compensator.

1.4.2 Specific objectives

1. Design and fabricate a Parabolic Dish Solar Concentrator.
2. Design and fabricate a receiver with a thermal compensator.
3. Design and fabricate a manual solar tracker
4. Determine the Efficiency η and Concentration ratio C for the system.

1.5 Literature Review

It is estimated that the total solar energy received by the earth annually is about $1.7x10^{17}$ W (Saperstein, 1975; Beggs, 2009). This is a large amount of energy that is estimated to be about 18 times that of the current primary energy demand. However, only 18% of the worlds energy demand is supplied from renewable energy sources, one of which is solar power. In the U.S.A, the world's leading country in renewable energy production; only 7% of its energy demand is generated from renewable sources with the rest coming from petroleum, natural gas, coal, and nuclear power in the order of decreasing dependency as depicted by Figure 1.2 (Classroom energy, 2014). Even with today's higher energy costs, the nonrenewable energy sources are generally more reliable, affordable and easier to store and transport than renewable energy resources (Gilbert, 2004). For renewable energy use to become more widely used, many technical hurdles must be overcome. Most hurdles have to do with the efficiency of tapping renewable energy, as well as producing and distributing this resource more reliably and economically (Classroom energy, 2014; USDOE, 2014).

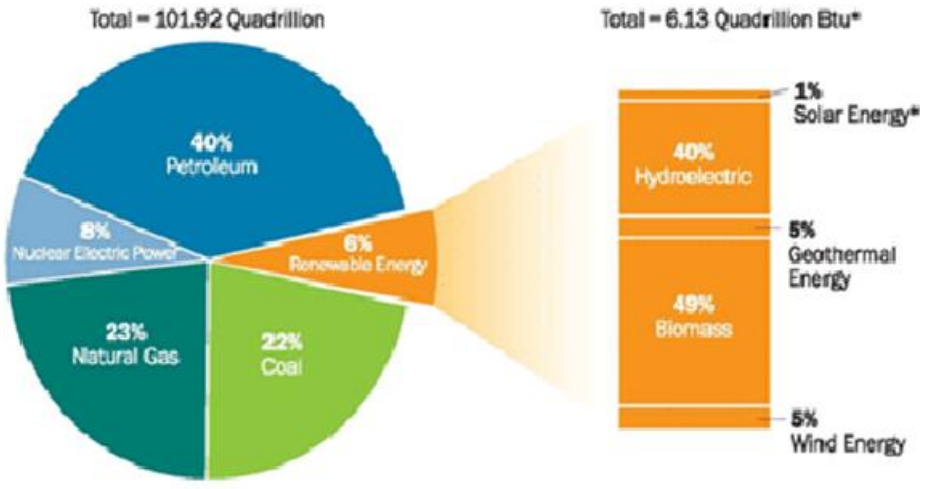

Figure 1.2: Energy mix in the U.S.A [Source - Classroom energy 2014]

The major reason for the low level of exploitation of solar energy is because solar flux is dispersed in nature, intermittent, unpredictable and only available during the day. The other prohibiting factor is the high capital investment required in construction and solar tracking cost of solar harvesting devices. A solution to mitigate the looming energy crisis resulting from overuse of finite primary energy sources is to develop affordable solar thermal concentrators. Various methods have been used across the world to intercept solar thermal radiation such as the flat plate collectors, Fresnell reflectors, parabolic trough and the parabolic dish (Harvey, 2010). By and large, the parabolic dish has been found to be more efficient and able to attain substantially high temperatures (Price, Lufert, & Kearney, 2010). Aluminium is the most widely used reflective material because it has considerably high reflectivity (0.96) within the whole electromagnetic spectrum, Figure 1.3 (Wackelgard, Niklasson, & Granqvist, 2001) Aluminium is also relatively cheap, easier to forge, and weather resistant.

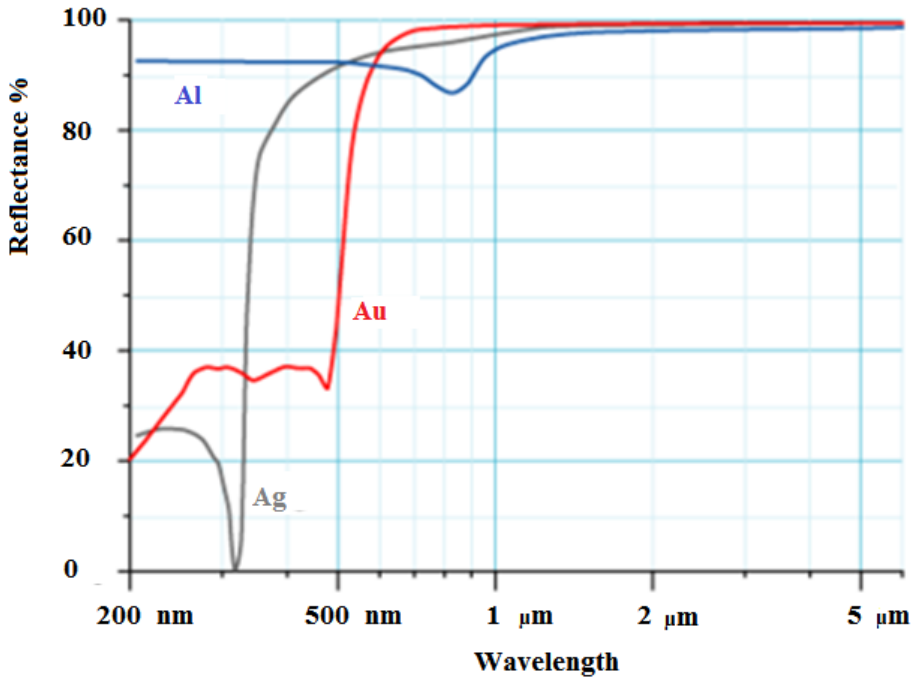

Figure 1.3: Spectral reflectance curves for aluminium (Al), silver (Ag), and gold (Au) metal mirrors at normal incidence (Orel, Gunde, & Hutchins, 2002)

A spherical solar concentrator has been developed (Medved, Meglic & Novak, 2009). This suffers the setback of spherical aberration resulting to low efficiency. A near-ideal solar thermal concentrating system is capable of extracting an amount of energy that is 90 % of the one incident at the surface (Thomas & Goldenberg, 1993).

In the study done by Mridul, (2006) on Parabolic dish design and fabrication, the construction design failed to maximize solar flux intercepted by the aperture due to shading caused by receiver support.

A study by Kawira, (2011) developed a Parabolic solar concentrator with a line focus. In the study, the reflectances of different types of aluminium sheets were determined and results obtained as follows: Aluminium metal sheet (0.83), Car solar reflector (0.81), Aluminium foil (0.78), and Gift wrapper (0.76). They found that aluminum foil has lower reflectance compared with aluminium metal sheet and car reflector but it serves a good trade-off because it is cheap and easy to fabricate.

1.6 Theoretical background

Direct solar radiation enters the atmosphere at the rate of 1370 W/m^2 at air mass zero (AM 0) with 65% to 75% of the radiation reaching the surface of the earth at about 1000 W/m^2 according to World Radiation Centre, WRC (Gillet, 1985). Solar flux is usually a continuous spectrum of wavelengths ranging from 0.25μm to about 2.4 μm, Figure 1.4. Fractions of intensities of various wavelengths given by the solar spectral distribution at air mass 1.5 (AM 1.5) are shown in Figure 1.5. It is evident from the distribution curve that the highest intensity of irradiance is in the region of visible spectrum ($0.38\mu m < \lambda < 0.78\mu m$). This accounts for a fraction of 0.48 of the total radiation. The wavelengths greater than 0.78μm is infrared and accounts for a fraction of 0.483 of the total radiation (Marion, 1994). Applying these fractions to the solar constant of 1000 W/m^2 at the earth's surface and considering the conversion from short wave radiation to long wave radiation through reflection, a proportion of about 0.963 of

radiant heat can be harnessed from the sun (Orel *et al.*, 2002). SolarGIS database on solar performance depict Kenya as one of the regions that receives a lot of insolation most part of the year, Figure 1.6.

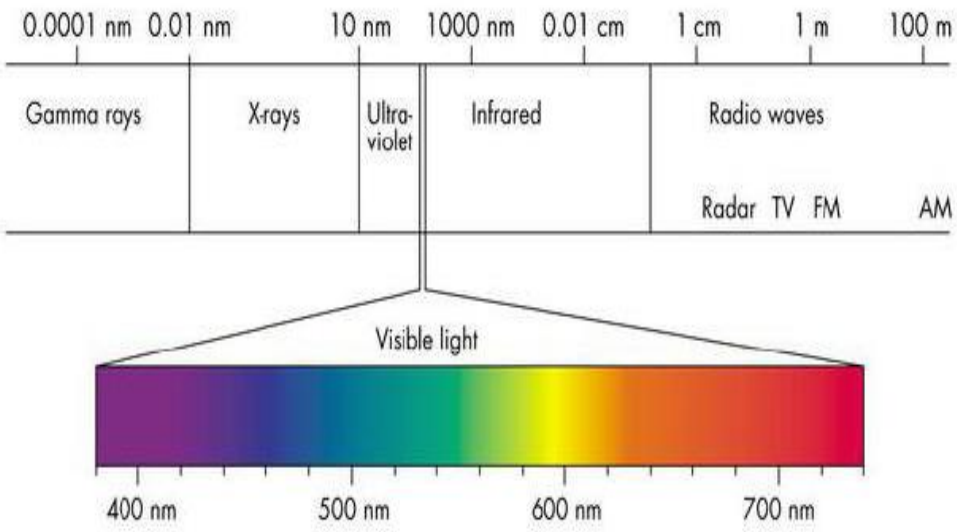

Figure 1.4: Part of the Electromagnetic Spectrum (WRDC)

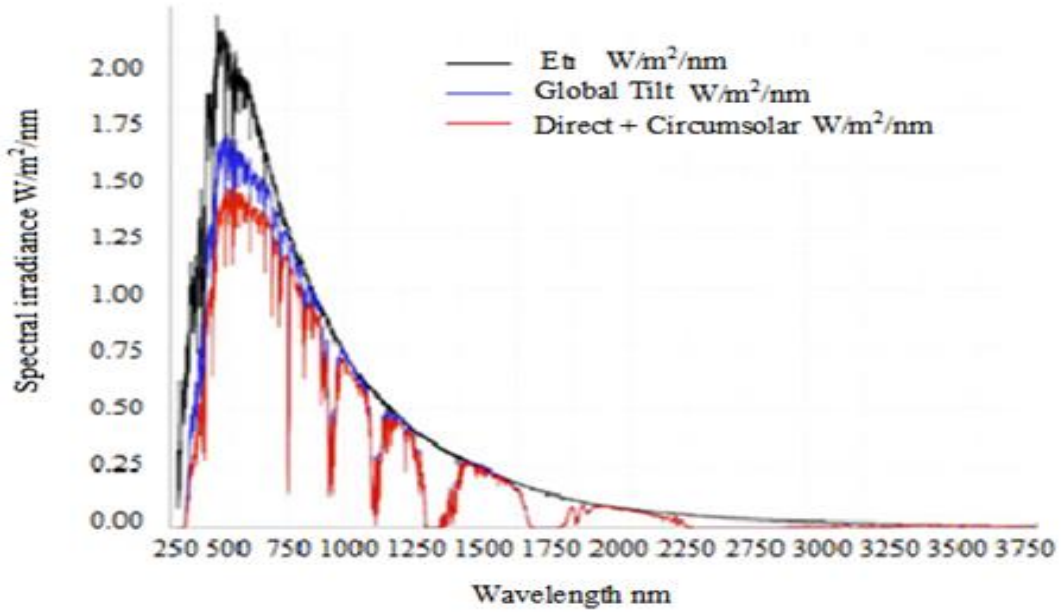

Figure 1.5: Solar spectral distribution at AM 1.5 (ASTMG173-03 Reference Spectra)

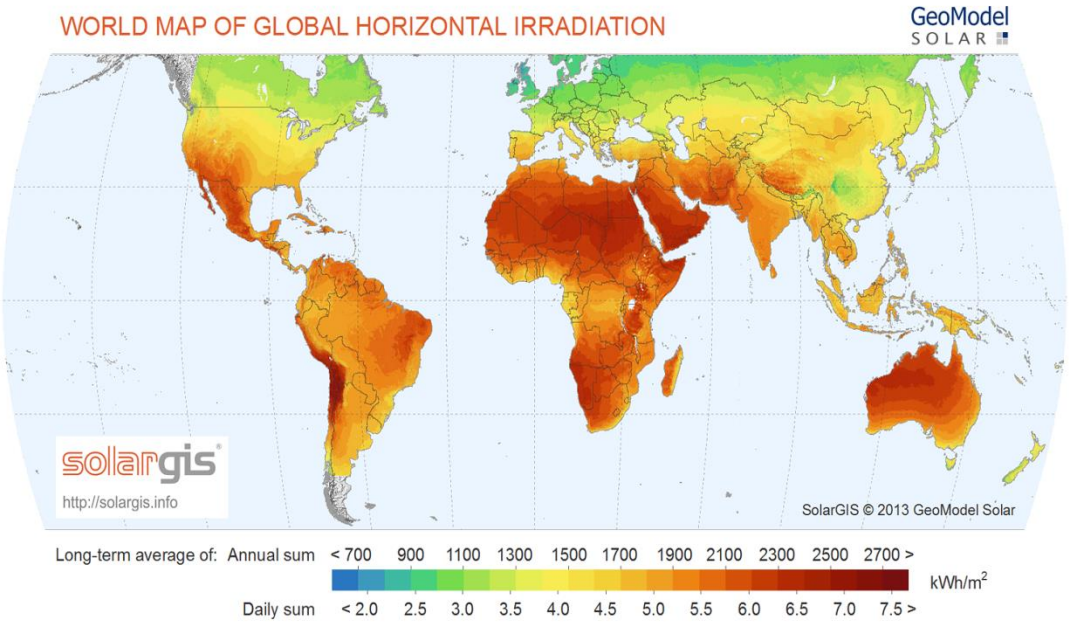

Figure 1.6: Global solar energy mapping (SolarGIS)

Solar energy and renewable energy in general is a dispersed form of energy and its harvesting and usage is faced by two main challenges which are: concentration and storage of energy (Rai, 1987; Price *et al*., 2010):

1.6.1 Concentration of Energy

Dispersed energy flux must be concentrated in order to meet the end use requirement that is compatible with conventional energy sources. Concentration refers to increasing the energy density of intercepted beam by reflecting it to a smaller area (Bill, 1980). By the laws of conservation of energy, there is always power loss whenever there is energy transfer or transformation. The choice of materials for solar thermal concentrators should guarantee minimum energy loss while at the same time being within a cost-effective range. Various designs such as the spherical reflector, Fresnel's reflector, parabolic trough and the parabolic dish have been used in intercepting and concentrating solar energy. The parabolic dish reflector has been found to be more efficient and able to attain substantially high temperatures at high concentration ratios (Price *et al*., 2010). Aluminium also has a wide variety of cheaper reflectors which can be used mounted on correct substrate, (Rai, 1987; Kawira, 2011). Scratches, pits, dust and polishing marks on a reflecting system can cause angle scattering of incident solar radiation and therefore the reflecting surface should be as smooth as possible.

The intercept, γ is defined as the fraction of radiation that reaches the absorber after reflection by the reflective dish. A high intercept factor is achieved by good dish geometry, smooth reflective surface and proper dish orientation. This maximizes the proportion of the reflected beam reaching the absorber. The absorber must be of reasonable surface area. Too small surface area may not capture stray beam missing the focus and on the other hand a very large surface will reduce the concentration ratio. High concentration ratios of between 600 - 2000 have been achieved with Parabolic Dish Reflectors (PDR) with different characteristics of the central receiver (Cengel, 2003).

Concentration ratio is the ratio of surface area of collector aperture to the surface area of the receiver. It is given by,

$$C = \frac{A_a}{A_r} \qquad \text{..... 1.1}$$

where A_a and A_r are areas of collector aperture and receiver respectively.

1.6.2 Energy Storage

Solar energy flux is only available during the day and more so when the sky is clear. Intensity of solar radiation fluctuates erratically both seasonally and diurnally depending on the weather condition and time of the day, with maximum intensity occurring at solar noon. Figures 1.7(a) and 1.7(b) show typical diurnal variations of global solar radiative flux in the equatorial region. Figure 1.7(a) shows a cloudless atmosphere and Figure 1.7(b) shows the impact of clouds.

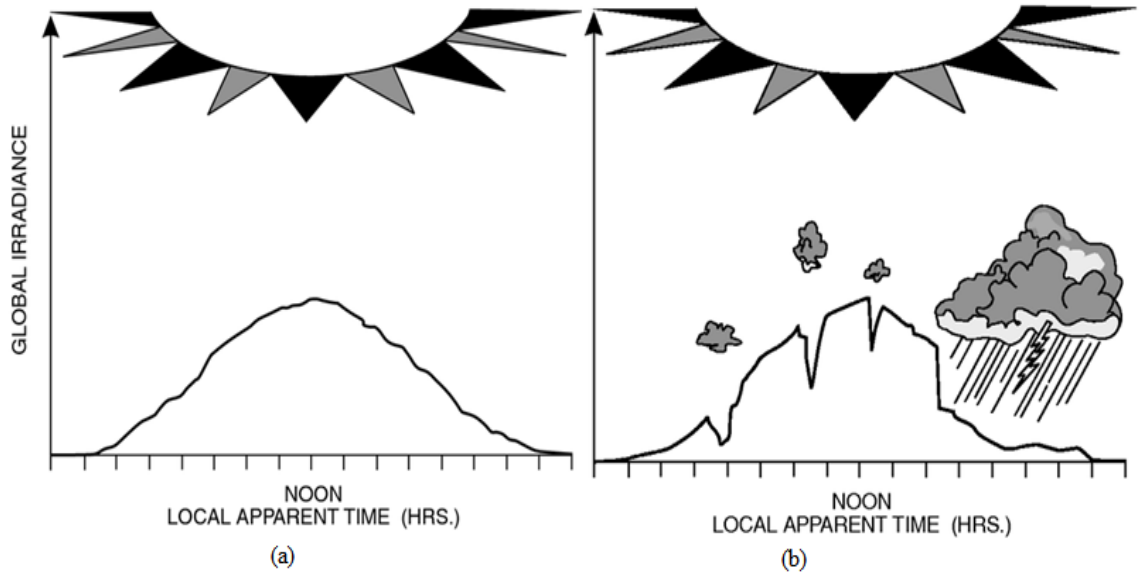

Figure 1.7: Diurnal variations of global solar radiative flux on (a) sunny day (b) cloudy day in the equatorial region. (https://www.newport.com/Introduction-to-SolarRadiation/411919/1033/content.aspx)

Solar energy can only be useful during absence of radiation if there is appropriate heat storage and recovery mechanism. The heat capacity of the materials making the receiver may be very small owing to the small size of the absorber. Any compensation of energy to make up for lost heat during shade is therefore negligible. There arises the need to have temporary energy storage so as to give a steady energy supply in the absence of intense solar radiation (Ari, 1985). This is an expensive undertaking because it requires large quantities of matter with high specific heat capacity or high latent heat of fusion, where phase change materials (PCMs) are used. Thermal energy storage can be classified by storage mechanism (sensible, latent or chemical) or by storage concept (active or passive). Thermal storage can utilize sensible or latent heat mechanisms or heat coming from chemical reactions. Sensible heat is the means of storing energy by increasing the temperature of a solid or liquid. The latent heat, on the other hand, is the means of storing energy via the heat of transition from a solid to liquid state for melting process or transition from liquid to gas for vaporizing materials. The comparison between latent and sensible heat storage shows that when latent heat storage is used, storage densities of 5 to 10 times higher can be achieved (Energy Technology Systems Analysis Program, 2013). High volumetric heat capacity is desirable because it leads to lower storage system size, reducing the structural costs and enhancing the energy concentration ratio.

Thermal energy can be stored in the sensible heat (temperature change) of substances that experience a change in internal energy. The stored energy is calculated by the product of its mass, the average specific heat, and the temperature change. Besides the density and the specific heat of the storage material, other properties are important for sensible heat storage which includes: operational temperatures, thermal conductivity and diffusivity, compatibility among materials, chemical and physical stability and cost (Hale *et al.*, 1971; Garg *et al.*, 1985; Buddhi *et al.*, 1994)

Various thermal storage media have been employed in heat storage and recovery systems. Thermal storage using water tanks uses the advantage of the high heat capacity

of water as compared to other sensible heat storage materials. Hot water in well lagged and polished tanks can take a considerable duration of time before cooling such that heat stored can be utilized at a later time (Duffie, 1991). Thermo-chemical heat storage in Glaumber's salt is a mechanism in which the heat storage material is a hydrated salt which loses the water of crystallization in a heat-seeking (endothermic) reaction (Fernanda, 1988). The same quantity of heat is released when the salt becomes hydrated in a heat-releasing (exothermic) reaction. The commonly used salt is hydrated sodium sulphate, $Na_2SO_4 .10H_2O$ or hydrated calcium chloride, $CaCl_2.6H_20$ (Lane, 1983)

$$Na_2SO_4 .10H_2O \longrightarrow Na_2SO_4 + 10H_2O \quad +\Delta H \text{ J}$$

Then

$$Na_2SO_4 + 10H_2O \longrightarrow Na_2SO_4 .10H_2O \quad -\Delta H \text{ J}$$

Phase changing materials (PCM) make use of the latent heat of fusion/vaporization of salts or metals (Sayigh, 1979). As the temperature rises, the chemical bonds within the PCM break up as the material changes from solid phase to liquid phase. This is a heat-gaining process while the bond formation (liquid phase to solid phase) is a heat-releasing process which helps in the heat recovery process.

The ability to store thermal energy is given by,

$$A = \frac{Q_s}{V} = \frac{mC_p \Delta T}{V} = \rho C_p \Delta T \qquad \text{..... 1.2}$$

where m is the mass of storage material in kg, Q_s is thermal energy calculated from the heat capacity, V is the volume in m^3, ρ is the density in kg/m^3.

Latent heat storage (LHS) is more attractive than sensible heat storage (SHS) because it is possible to store larger amount of heat with only small temperature changes. LHS therefore has a high storage density mechanism. The change of phase occurs

isothermally and takes some time to complete, making it possible to maintain constant temperature (Lane, 1983; Abhat, 1983). LHS therefore has the ability to maintain near isothermal conditions during the heat recovery process. However, many practical problems are encountered with LHS due to low thermal conductivity and variation in thermo-physical properties under extended cycles of phase transition.

The choice of a good PCM depends on technical aspects particular to the solar energy device (Hale *et al.*, 1971; Garg *et al.*, 1985; Buddhi *et al.*, 1994). However a good PCM should have desirable characteristics. It should have high latent heat effect, i.e., high latent heat of fusion per unit volume such that the required volume of the container to store a given amount of energy is relatively small. The phase change must be reversible over very large number of cycles without degradation, with the melting point being in the desired operating temperature range. High specific heat capacity provides for additional and significant sensible heat storage.

High thermal conductivity of PCM in both solid and liquid phases provides good thermal contact for effective charging and discharging of energy. It should have small volume changes upon phase transformation and small vapour pressure at operating temperatures so as to reduce the containment problem. The material must be chemically stable and non-toxic, non-corrosive to the construction materials and of reasonable cost (Sharma, 1999). Table 1.2 shows various PCMs and their properties.

Physically and chemically stable salts that are cheap and readily available such as sodium chloride (NaCl) have been used as thermal storage materials though at a reservoir away from the receiver (Tiwari, Rai, & Santram, 1988). The compounds have low mass density necessitating huge volumes of material which cannot be accommodated at the receiver. A proportion of thermal energy is lost during transportation of the heat transfer fluid to the reservoir thus compromising efficiency. Furthermore such stable ionic compounds melt at elevated temperatures e.g. sodium

chloride, NaCl (802 ^{o}C), magnesium chloride, $MgCl_2$ (800 ^{o}C) which are unattainable in the moderate temperature concentrators.

Table 1.2: Properties of some PCMs [Hale, Hoover, & O'Neill, 1971; Lane, 1983; Garg, Mullick, & Bhargava 1985; Buddhi & Sawhney, 1994; Sharma, 1999; Gustafsson, Bo & Seterwall, 1998; Zalba, Marin, Cabeza & Mehling, 2003; Farid, Khudhai & Razacksak, 2004]

Name of material	Melting point (^{o}C)	Density (kg/m^3)	Latent heat (kJ/kg)
Orthophosphoric acid $H_4P_2O_6$	55.0		213
Dintro toluene (2,4)	70.0		111
Tin trichloride	73.4		25
Phenylacetic acid	76.7		102
T Benzylamine 78.0 174hiosinamine	77.0		140
Durene	79.3	838	156
Acetamide	81	1159	241
Alpha napthol	96	1095	163
Glautaric acid	97.5	1429	156
Methyl Fumarate	102	1045	242
Catechol	104.3	1370	207
Quinone	115	1318	171
Acetanilide	115	1210	142
Succinic anhydride	119	1104	204
Benzoic acid	121.7	1266	142.8
Stibene	124	1164	167
Benzamide	127.2	1341	169.4
Alpha glucose	141	1544	174
Salicylic acid	159	1443	199
O-Mannitol	166	1489	294
60Sn40Pb alloy	172	8520	23
Hydroquinone	172.4	1358	258
Potassium hydroxide - Zinc chloride	190	2060	230.6

Mixture (64:36)

Name of material	Melting point (^{o}C)	Density (kg/m^{3})	Latent heat (kJ/kg)
Zinc chloride	283	2900	168.8
Sodium nitrate	307		199
Sodium hydroxide	319	2260	171.8
Potassium nitrate	380		266
Potassium hydroxide	380		149
Magnesium chloride	800		492
Sodium carbonate	854		275
Potassium fluoride	857		452
Potassium carbonate	897		235

The 60Sn/40Pb alloy which is a eutectic mixture that melts at 172^{o}C can be considered because it is within the attainable temperature range of the prototype PDSC. Although the alloy has relatively lower specific latent heat of fusion compared to other alternatives cited here, it has the advantage of high mass density and hence can act as a good thermal reservoir. It also has better thermal conductivity which enhances heat transfer. At optimum operating temperature the PCM is in the liquid state and thus preserves the latent heat of fusion and a buffer temperature can be established as the cooling curve of SnPb shows in Figure 1.8. This acts as a thermal compensator and when incorporated at the receiver can address the SED problem of smoothing out energy output.

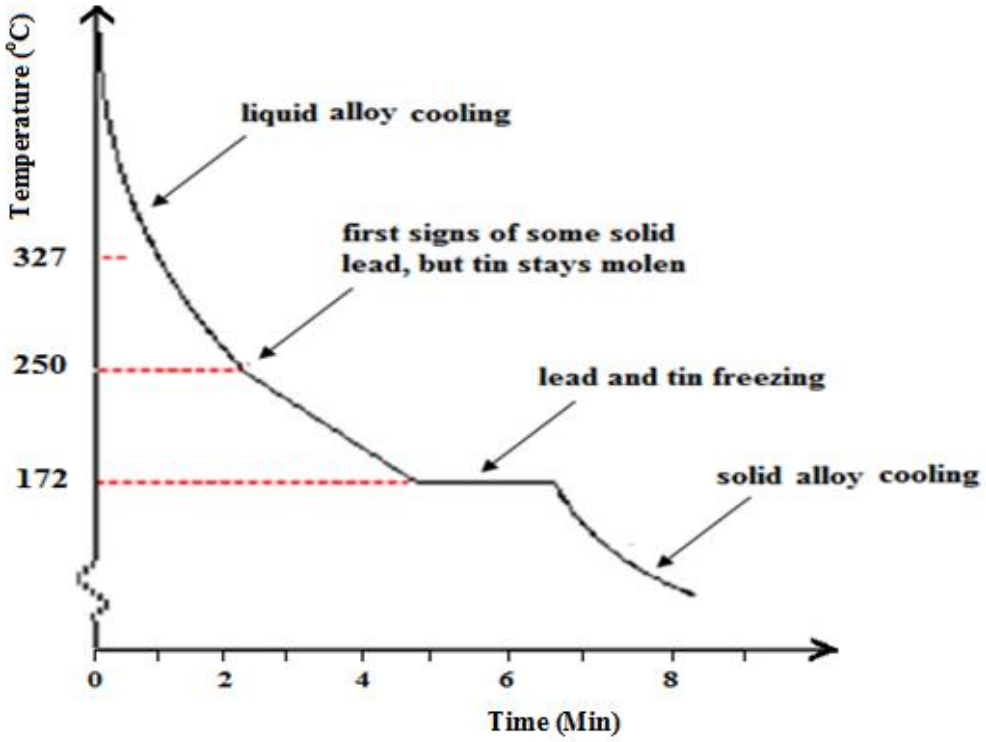

Figure 1.8: Cooling curve of 60Sn40Pb alloy (chemguide.co.uk)

The two challenges of energy concentration and storage have a bearing on efficiency (Christopher, Martin, & Yogi, 2005). The first law of thermodynamics defines efficiency, η_1 as the ratio of useful output energy of a device to the input energy of the device.

$$\eta_1 = \frac{\text{usefuloutput energy}}{\text{energy output}} \quad \text{.....} \quad 1.3$$

Efficiency is optimized by maximizing the thermal energy captured to ensure that the greatest proportion of solar beam is reflected to the absorber and that minimum loses occur during the transfer. The absorber must be of good absorbance and thermal conductivity in order to effectively transport heat energy to the heat transfer fluid. Most absorbers are made of blackened zinc which has good absorptance and good thermal conductivity (Geyer, 1991). However, zinc is relatively expensive and therefore wrought

iron which is cheaper and of appreciably good thermal conductivity can serve as a good trade off. The rate of heat loss of the absorber is proportional to its surface area according to Stephan-Boltzmann law of black body radiation, equation 1.4 and therefore the absorber area should be small enough compared with the dish aperture area.

$$\dot{Q} = \sigma A T^4 \quad \text{.....1.4}$$

where $\dot{Q}$ is rate of heat loss, σ is Stephan's constant, A is the area and T is the absolute temperature.

Solar tracking is inevitable for optimum performance of PDRs. A normal radiation beam is reflected to the focus of the paraboloid but rays entering the aperture at a different angle deviate from the focus. Most tracking devices use electronic mechanisms that are operated by external power which not only increases the outlay cost but also reduces the overall efficiency. Manually tracked PDSC can mitigate installation and running cost of the SED. Steam generating PDRs have the challenge of thermal losses during transportation of heat to the converter or storage media (Kelly & Lessley, 1994). Every energy transformation is accompanied by some energy loss and hence the need to harvest solar energy through the most direct end use process. Figures 1.9 and 1.10 illustrate possible energy transformation pathways.

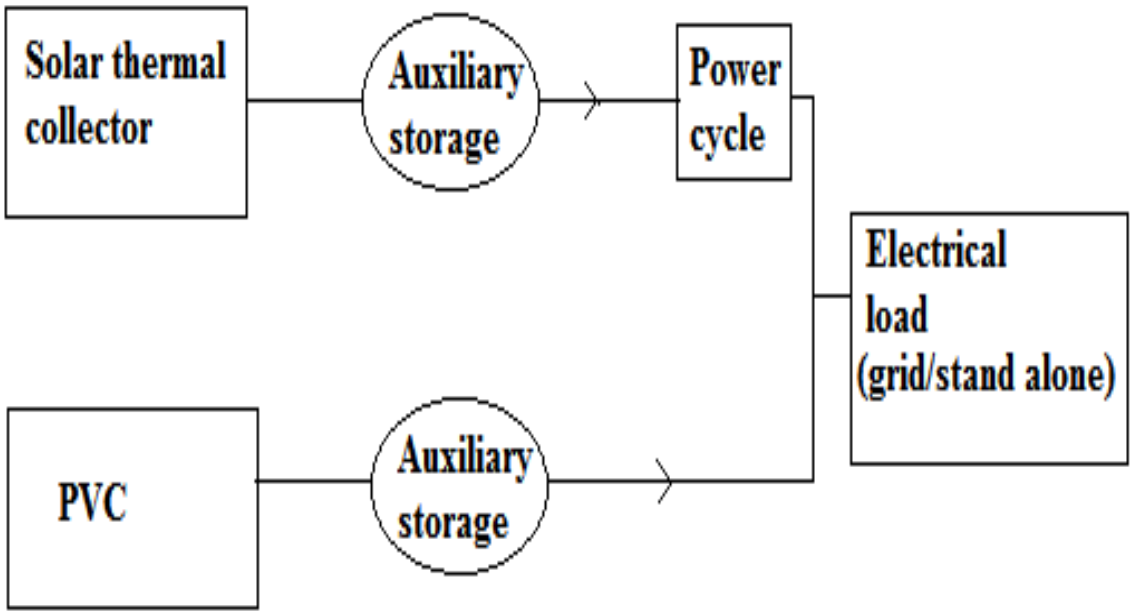

Figure 1.9: Schematic flow diagram representing solar energy transformations

In Figure 1.9, solar thermal energy is collected at the harvesting point and then temporary stored in the auxiliary storage device in the form of latent or sensible heat. The heat energy is them converted to mechanical and electrical energy in the power cycle chamber. In the photovoltaic cell (PVC) pathway, the solar cell converts solar energy to electrical energy. This energy is stored in chemical form using batteries before being reconverted to electrical energy at the time of need. The transducers at every stage of transformation dissipate energy thus reducing the overall efficiency. Likewise in a domestic hot water system shown in Figure 1.10, heat energy must be buffered in order to give a constant supply during use. There are always heat losses through conduction, convection and radiation of the PCM.

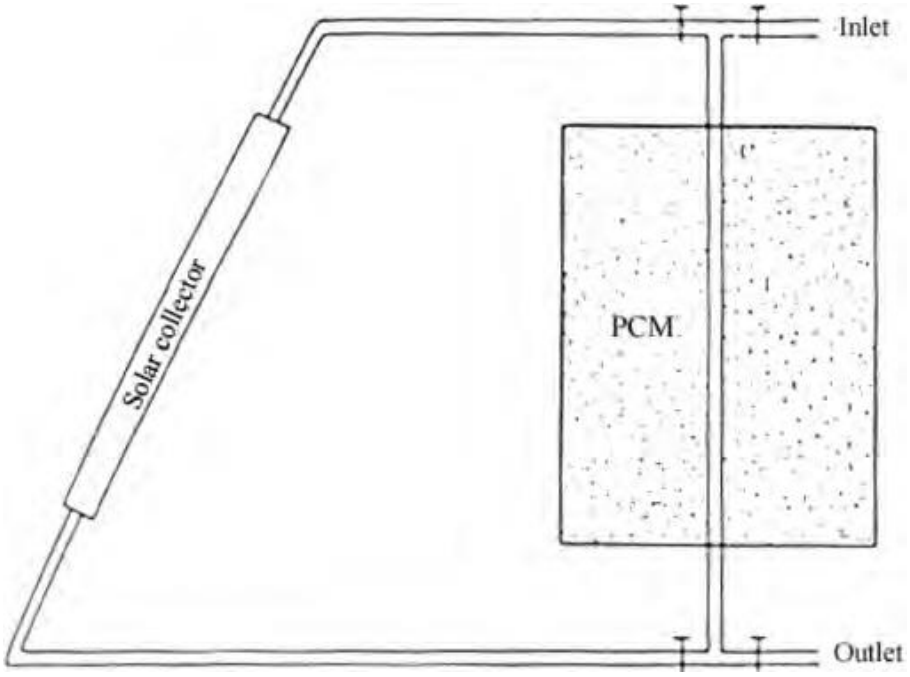

Figure 1.10: Domestic hot water system with separate latent heat storage unit.

Recent PDR systems for generating electricity are designed with the steam turbine generator at the central absorber which in turn requires a large area hence reducing the concentration ratio. A high density thermal storage medium at the absorber can smooth out energy output while solving the problem of heat loss during transportation.

1.6.3 Improvements on SEDs

The cost of the suggested PDSC will be within affordable levels since some of the materials used are recycled and readily available. The thermal compensator component makes the device reliable because it gives steady energy output solving the problem of inconveniences caused by fluctuations of solar energy. The compensated PDSC is expected to be more efficient than non-compensated PDSCs of similar dimensions

CHAPTER TWO

MATERIALS AND METHODS

2.1 Study area

The study was done in an open area at Jomo Kenyatta University of Agriculture and Technology in Juja, Kenya located at geographic coordinates 1^{o} 11'S and 37^{o} 7'E.

Figure 2.1: Geographical location of the study area [Google maps 2015].

2.2 Procedure

The construction was done in three stages beginning with the dish, the receiver and the manual tracker (see Plate A5). The three components were then assembled and the system positioned along the N-S axis so as to track the sun along the equatorial latitude.

A tilting mechanism was put in place to take care of the solar declination angle during the solar harvesting season for higher intercept factor.

The prototype dish operates by intercepting direct solar flux and reflecting it using aluminium kitchen foil to a receiver at the parabolic focus. The receiver was a blackened metal bulb containing an alloy of a low melting point surrounding a coiled copper tube. The copper tube carried water as the Heat Transfer Fluid (HTF). To achieve a high concentration ratio, a small size receiver was used to ensure small surface area relative to the dish aperture area. On a clear day the operating temperature of the receiver would go above the melting point of the alloy thus storing latent heat and also sensible heat. During transient cloud cover the cooling alloy would lose the sensible heat and release latent heat of fusion to the HTF thus compensating for the absent solar energy. There would therefore be a time lag in temperature swings due to erratic weather conditions. The 60Sn40Pb alloy is an eutectic mixture with a fixed melting point of 172 ^{o}C and latent heat of fusion of 2.3 x 10^4 J/kg. At a regulated flow rate of HTF, the heat capacity of the PCM and latent heat of fusion would transfer heat to the flowing water maintaining a buffer temperature that makes the system to smooth out energy output. A solar tracking mechanism consisting of a helical spring of appropriate stiffness was employed to store elastic mechanical energy and release it during unwinding. A braking mechanism was devised to control the unwinding speed as shown in Plate A2.

2.2.1 Fabrication of Parabolic Dish

The Parabolic Dish shape was done by first considering the equation of a parabola and sketching it on a horizontal surface as shown in Plate 2.1 and Figure 2.1.

The standard equation of a parabola is,

$$y = ax^2 + bx + c \quad \text{.....2.1}$$

where a, b and c are constants

The simple form of the equation is,

$$y = ax^2 \qquad \text{……...……..…2.2}$$

where the vertex is at (0, 0) and symmetry is on the y-axis.

In the prototype dish the equation was

$$y = \frac{1}{360} x^2 \qquad \text{……..……2.3}$$

The focus of the parabola is given by

$$f = \frac{1}{4a} \qquad \text{……2.4}$$

Where the coefficient, $a = \frac{1}{360}$

The focus was 0.90 m from the base of the dish.

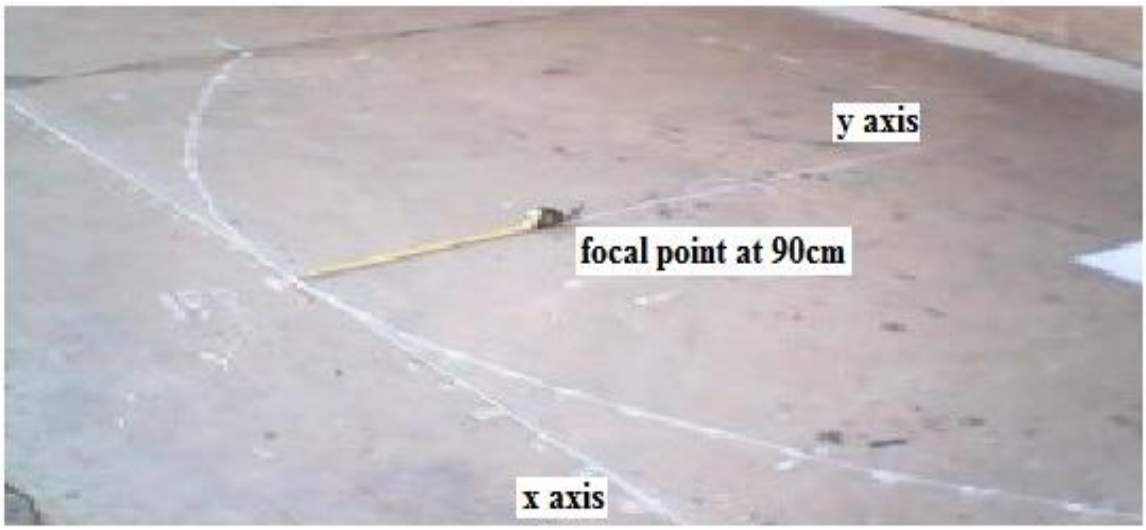

Plate 2.1: Calculation of dish geometry

Four steel rods were curved to take the shape of the parabola and then welded together at their vertices before joining the ends with a circular ring as show in figure 2.3. The diameter of the aperture was 3.0 m giving aperture area of 7.07 m^2.

A circular metal plate was welded at the vertex of the dish leaving a hole to allow the fitting of inlet and outlet tubes encased in a steel pipe. The parabolic surface was filled with 3-ply wood polished with varnish to make a water proof substrate. The inside surface was lined with aluminium kitchen foil fitted with adhesive paste as illustrated in Figure 2.2 and Plate 2.2.

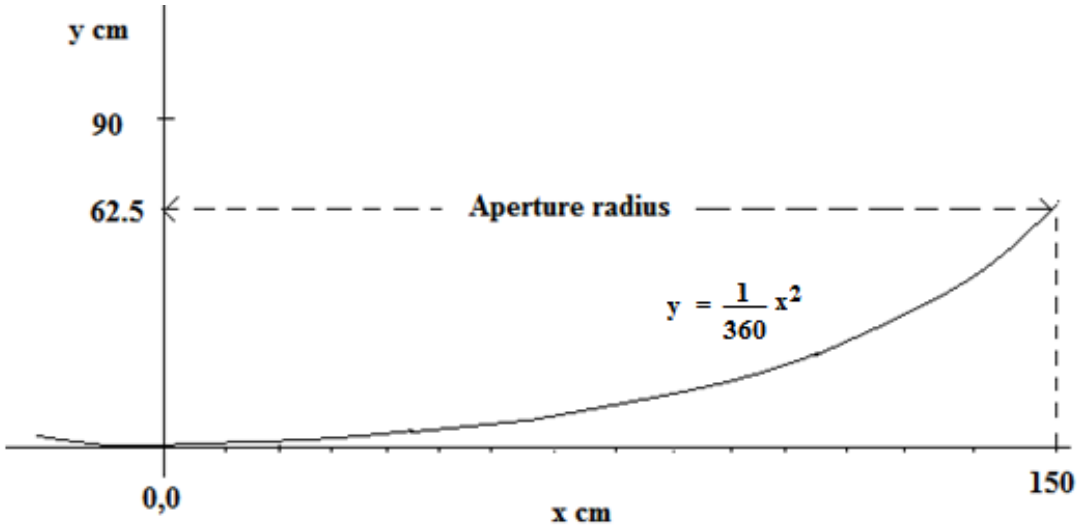

Figure 2.2: Geometry of the Parabola

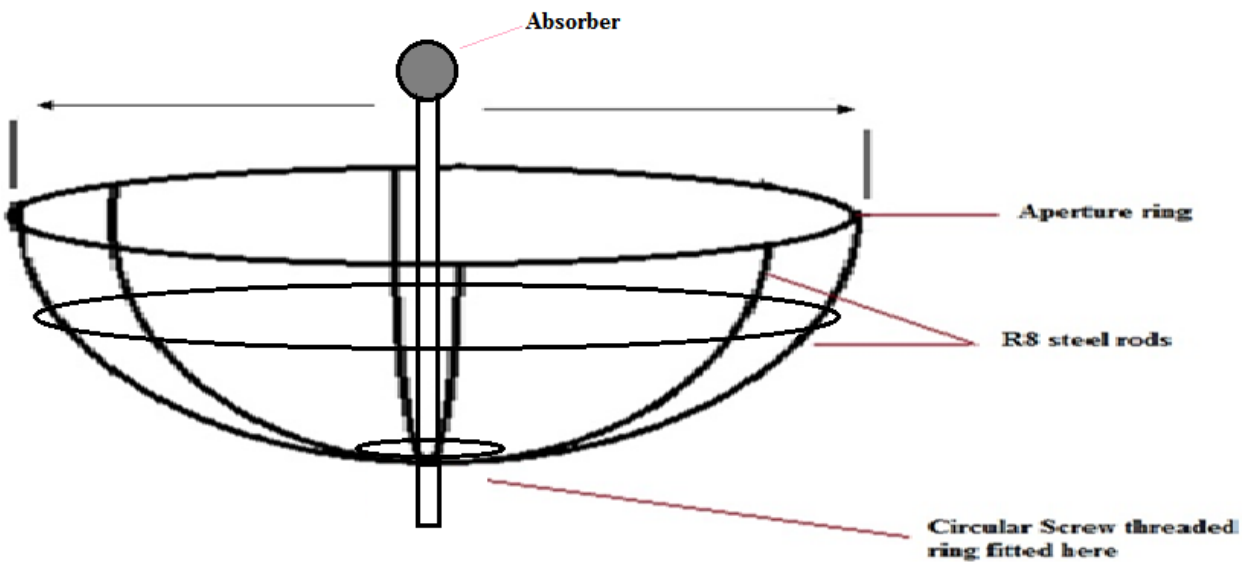

Figure 2.3: Parabolic dish fabrication

Plate 2.2: Parabolic substrate

2.2.2 Fabrication of the Absorber

The absorber was constructed using a steel globe salvaged from an obsolete refrigerator compressor unit. This served as the blackened bulb absorber, housing the PCM of Sn/Pb alloy. The PCM surrounded a coiled copper tube as shown in Plate 2.3, carrying the HTF which was water in this particular case. The inlet narrow pipe was insulated from the outlet steam pipe with glass wool to prevent heat exchange as show in Figure 2.4. The mass of alloy at the absorber was 2.65 kg and the radius of the absorber was 6.5 cm. The absorber was accurately fixed at the focal point of the dish where the reflected solar beam converges.

Plate 2.3: Construction of Absorber before enclosing it

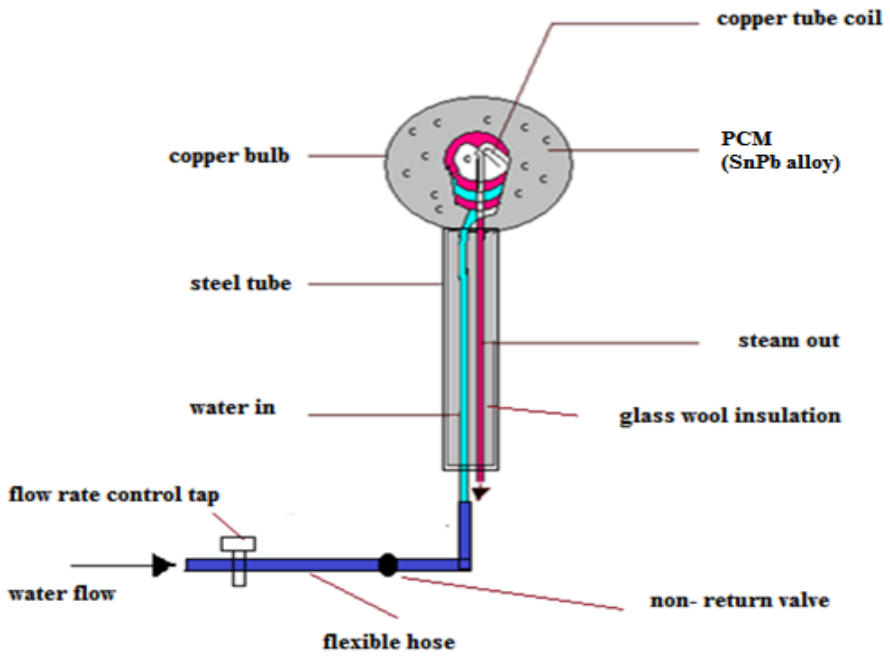

Figure 2.4: The absorber assembly

The Parabolic Dish and the Absorber assembly were then mounted on a horizontal axis support comprising the manual solar tracker. Figure 2.5 is a representative diagram illustrating the features of the PDSC and Plate 2.4 shows the complete dish assembly (see also Plate A6).

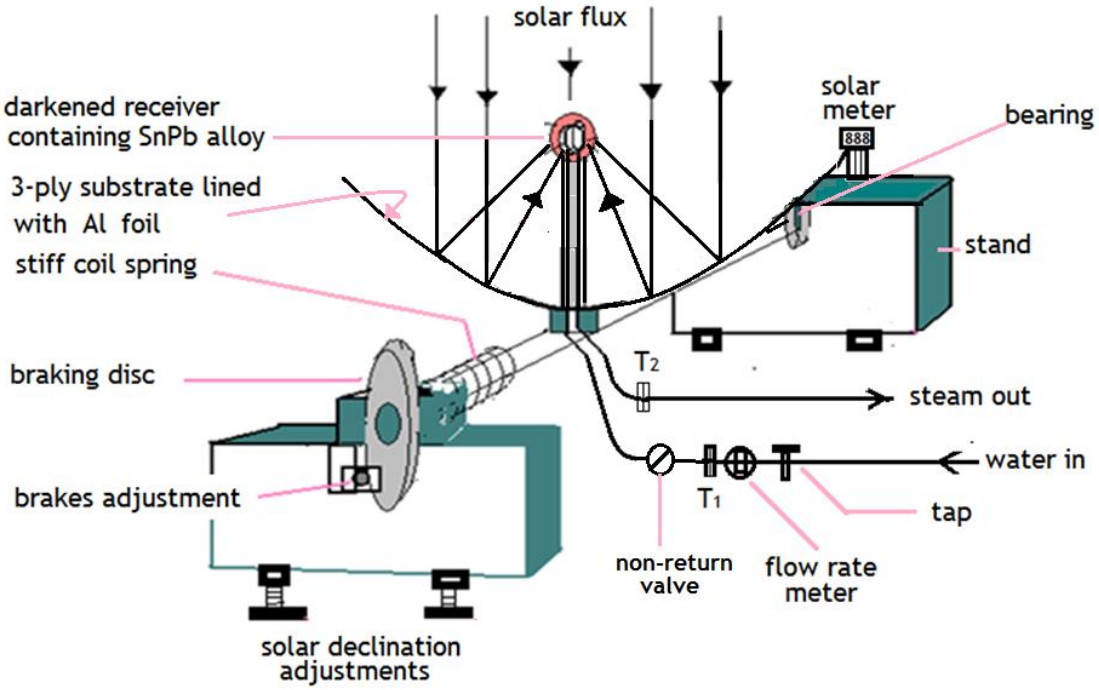

Figure 2.5: Complete PDSC assembly

Plate 2.4 shows the dish reflector surface of aluminium foil lined on the substrate, which is pivoted on an axle that spins on top of two drums that serve as stands. The dish is inclined at the solar declination angle so that the aperture intercepts radiation beam at 90^{o}.

Plate 2.4: The complete PDSC intercepting the solar beam

2.2.3 Positioning of the PDSC

The solar harvesting device was located at an open area away from tall obstacles such as trees and buildings which would otherwise obstruct radiation and in effect reduce the solar harvesting period. The location of experiment was free from interference of shadows only after 09.00 hrs. The sun-rising and setting direction was determined prior to the experiment. This was done using a straight rod fixed perpendicular to a wooden board which was placed horizontally on a level ground. The length of shadow vectors cast on the board were measured between 09.00 hrs to 16.00 hrs at 30 minutes interval. Each vector was projected the same length backwards from the base of the vertical rod. The second position vector represented the locus of the sun at various times of the day.

The locus of the sun was found to be a straight line and its direction was measured using a magnetometer. The direction of the sun was found to be 3^oS of E to 3^oN of W. It was from this fact that the PDSC was mounted with its rotational axis being perpendicular to the solar direction so that the dish aperture would tilt along the direction of the sun.

2.2.4 Solar declination angle, δ

The angle between normal and the solar beam when the sun is at zenith is the solar declination angle. This angle varies with seasons of the year between 30^o north of equator and 30^o south of equator when the sun is in the northern hemisphere and southern hemisphere respectively. The SED was a single axis tracking system which is prone to inefficiencies due to cosine losses. Cosine losses result from failure of reflected beam to focus on the absorber when the intercepted beam is not perpendicular to the dish aperture. In this study, it was assumed that the solar declination would have minimal variation within the short period of solar data collection. The dish was therefore inclined such that the aperture plane could capture the solar beam at 90^o. The solar declination angle was calculated using equation 2.5.

$$\delta = 23.4 \sin\left[\frac{360(284+n)}{365}\right] \quad \text{.....2.5}$$

where n is the day of the year.

The solar declination angle was determined on the 03/03/2014 which was the 62^{nd} day of the year. The calculated declination angle where n equal to 62 was found to be -7.5177^o

The solar declination angle was also determined using the method of shadows. A straight rod was fixed perpendicular to a plane that was hinged to a horizontal board. The movable plane was directed towards the sun such that when the sun was at zenith with respect to the plane, the shadow of the rod was of minimum length. The solar declination angle was measured between the movable plane and the horizontal plane

(figure 2.5) and was found to be -7.5^{o}. Therefore the dish was inclined at 7.5^{o} towards south because the sun was in the southern hemisphere during the season of experiment.

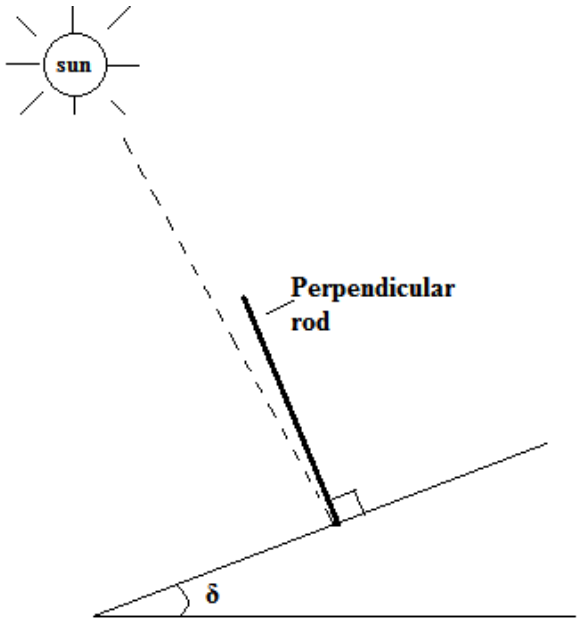

Figure 2.6: Determination of δ using the method of shadows

The declination angle obtained by the method of shadows was in close agreement with the mean values determined by SolarGIS database (Table 2.1) which gives the value as -7°03'

Table 2.1: Mean Value of the Solar Declination, δ for the Four Years of a Leap-Year Cycle of the Sun (SolarGIS database 2004)

Positive sign (+) Sun north of Celestial Equator; negative sign (-) Sun south of Celestial Equator.

Day	JAN	FEB	MAR	APR	MAY	JUN	JUL	AUG	SEP	OCT	NOV	DEC
1	-23°04'	-17°20'	-7°49'	+4°18'	+14°54'	+21°58'	+23°09'	+18°10'	+8°30'	-2°57'	-14°14'	-21°43'
2	-22°59'	-17°03'	-7°26'	+4°42'	+15°12'	+22°06'	+23°05'	+17°55'	+8°09'	-3°20'	-14°34'	-21°52'
3	-22°54'	-16°46'	-7°03'	+5°05'	+15°30'	+22°14'	+23°01'	+17°40'	+7°47'	-3°44'	-14°53'	-22°01'
4	-22°48'	-16°28'	-6°40'	+5°28'	+15°47'	+22°22'	+22°56'	+17°24'	+7°25'	-4°07'	-15°11'	-22°10'
5	-22°42'	-16°10'	-6°17'	+5°51'	+16°05'	+22°29'	+22°51'	+17°08'	+7°03'	-4°30'	-15°30'	-22°18'
6	-22°36'	-15°52'	-5°54'	+6°13'	+16°22'	+22°35'	+22°45'	+16°52'	+6°40'	-4°53'	-15°48'	-22°25'
7	-22°28'	-15°34'	-5°30'	+6°36'	+16°39'	+22°42'	+22°39'	+16°36'	+6°18'	-5°16'	-16°06'	-22°32'
8	-22°21'	-15°15'	-5°07'	+6°59'	+16°55'	+22°47'	+22°33'	+16°19'	+5°56'	-5°39'	-16°24'	-22°39'
9	-22°13'	-14°56'	-4°44'	+7°21'	+17°12'	+22°53'	+22°26'	+16°02'	+5°33'	-6°02'	-16°41'	-22°46'
10	-22°05'	-14°37'	-4°20'	+7°43'	+17°27'	+22°58'	+22°19'	+15°45'	+5°10'	-6°25'	-16°58'	-22°52'
Day	**JAN**	**FEB**	**MAR**	**APR**	**MAY**	**JUN**	**JUL**	**AUG**	**SEP**	**OCT**	**NOV**	**DEC**
11	-21°56'	-14°18'	-3°57'	+8°07'	+17°43'	+23°02'	+22°11'	+15°27'	+4°48'	-6°48'	-17°15'	-22°57'
12	-21°47'	-13°58'	-3°33'	+8°28'	+17°59'	+23°07'	+22°04'	+15°10'	+4°25'	-7°10'	-17°32'	-23°02'
13	-21°37'	-13°38'	-3°10'	+8°50'	+18°14'	+23°11'	+21°55'	+14°52'	+4°02'	-7°32'	-17°48'	-23°07'
14	-21°27'	-13°18'	-2°46'	+9°11'	+18°29'	+23°14'	+21°46'	+14°33'	+3°39'	-7°55'	-18°04'	-23°11'
15	-21°16'	-12°58'	-2°22'	+9°33'	+18°43'	+23°17'	+21°37'	+14°15'	+3°16'	-8°18'	-18°20'	-23°14'
16	-21°06'	-12°37'	-1°59'	+9°54'	+18°58'	+23°20'	+21°28'	+13°56'	+2°53'	-8°40'	-18°35'	-23°17'
17	-20°54'	-12°16'	-1°35'	+10°16'	+19°11'	+23°22'	+21°18'	+13°37'	+2°30'	-9°02'	-18°50'	-23°20'
18	-20°42'	-11°55'	-1°11'	+10°37'	+19°25'	+23°24'	+21°08'	+13°18'	+2°06'	-9°24'	-19°05'	-23°22'
19	-20°30'	-11°34'	-0°48'	+10°58'	+19°38'	+23°25'	+20°58'	+12°59'	+1°43'	-9°45'	-19°19'	-23°24'
20	-20°18'	-11°13'	-0°24'	+11°19'	+19°51'	**+23°26'**	+20°47'	+12°39'	+1°20'	-10°07'	-19°33'	-23°25'
Day	**JAN**	**FEB**	**MAR**	**APR**	**MAY**	**JUN**	**JUL**	**AUG**	**SEP**	**OCT**	**NOV**	**DEC**
21	-20°05'	-10°52'	**0°00'**	+11°39'	+20°04'	**+23°26'**	+20°36'	+12°19'	+0°57'	-10°29'	-19°47'	**-23°26'**
22	-19°52'	-10°30'	+0°24'	+12°00'	+20°16'	**+23°26'**	+20°24'	+11°59'	+0°33'	-10°50'	-20°00'	**-23°26'**
23	-19°38'	-10°08'	+0°47'	+12°20'	+20°28'	**+23°26'**	+20°12'	+11°39'	**+0°10'**	-11°12'	-20°13'	**-23°26'**
24	-19°24'	-9°46'	+1°11'	+12°40'	+20°39'	+23°25'	+20°00'	+11°19'	-0°14'	-11°33'	-20°26'	**-23°26'**

Day	JAN	FEB	MAR	APR	MAY	JUN	JUL	AUG	SEP	OCT	NOV	DEC
25	-19°10'	-9°24'	+1°35'	+13°00'	+20°50'	+23°24'	+19°47'	+10°58'	-0°37'	-11°54'	-20°38'	-23°25'
26	-18°55'	-9°02'	+1°58'	+13°19'	+21°01'	+23°23'	+19°34'	+10°38'	-1°00'	-12°14'	-20°50'	-23°23'
27	-18°40'	-8°39'	+2°22'	+13°38'	+21°12'	+23°21'	+19°21'	+10°17'	-1°24'	-12°35'	-21°01'	-23°21'
28	-18°25'	-8°17'	+2°45'	+13°58'	+21°22'	+23°19'	+19°08'	+9°56'	-1°47'	-12°55'	-21°12'	-23°19'
29	-18°09'	-8°03'	+3°09'	+14°16'	+21°31'	+23°16'	+18°54'	+9°35'	-2°10'	-13°15'	-21°23'	-23°16'
30	-17°53'		+3°32'	+14°35'	+21°41'	+23°13'	+18°40'	+9°13'	-2°34'	-13°35'	-21°33'	-23°12'
31	-17°37'		+3°55'		+21°50'		+18°25'	+8°52'		-13°55'		-23°08'

2.2.5 Solar noon

The local time of the day when the sun is right overhead (zenith) is the solar noon. Solar noon varies with the latitude and season (solar declination angle δ). On a clear day, this is the time when maximum solar flux would be expected. The solar noon was found by determining the time at which the shadow of a vertical rod fixed on a horizontal board was shortest. This time was found to be 01.30 hrs.

2.2.6 Flow rate and heat transfer

The HTF was delivered from a high tank reservoir and made to flow by gravity at a controlled rate so as to enter the high temperature focus. The delivery pipe was thin copper tube (diameter = 5mm) salvaged from an obsolete refrigerator. The narrow tube would ensure greater contact area and enough time for heat exchange. Good thermal contact was necessary for effective heat transfer thus copper was chosen for its good thermal conductivity. The rate of flow of HTF was measured using volume flow rate meter (Plate A3) and conversions done to mass flow rate ($\dot{m}$). A non- return valve in the inlet pipe was fixed to prevent counter flow of high pressure steam from the hot absorber but only allow it to proceed to the outlet. Two thermocouple thermometers were used to measure the inlet and outlet temperature (Plate A4). A third thermometer was used to

measure the ambient (environment) temperature. A solar power meter was used to measure prevailing solar beam radiation. The solar meter was Model No.: TM-206, with a 3½ digits LCD with maximum reading of 2000W/m^2, and a Data Hold/ MAX/MIN functions (see Plate 2.6 & Plate A1). The solar meter was fixed outside the aperture but perpendicular to the aperture plane and parallel to the antenna supporting the receiver as shown in plate A1. This would record the prevailing solar beam radiation intercepted by the dish aperture at various times of the day.

Plate 2.5: Model No.: TM-206 Solar meter.

Under steady state conditions, the temperature rise of water was used to determine the heat transferred to the water using the equation of heat gain:

$$\dot{Q} = \dot{m}c_p (T_2 - T_1) \quad \text{.....2.6}$$

where $\dot{m}$ is mass flow rate of the heat transfer fluid, c_p is the heat capacity of water at constant pressure, $(T_2 - T_1)$ is the temperature gradient with T_1 as the inlet temperature and T_2 as the outlet temperature of the heat transfer liquid and $\dot{Q}$ is the rate of transfer of heat or the power output (Twidell *et al.*, 1986).

The total heat intercepted by the dish was calculated using effective dish aperture area A_{ae} and the prevailing solar constant G_{sc}.

The effective aperture area was determined using equation 2.7

$$A_{ae} = A_a . r \quad \ldots\ldots 2.7$$

where A_a is aperture area and r is reflectance of aluminium foil = 0.78; A_{ae} is the effective aperture area.

In the prototype dish the effective aperture area was determined as:

$$A_a = 7.07 \text{ m}^2 \text{ x } 0.78 = 5.538 \text{ m}^2$$

The solar energy intercepted by the aperture area per unit time was calculated by:

$$\dot{Q}_s = G_{sc} A_a \cos \theta_i \quad \ldots\ldots 2.8$$

where G_{sc} is the prevailing direct solar intensity, θ_i is the angle of incidence. For the perpendicular aperture, $\cos \theta_i = 1$

A_a is a design parameter and was calculated from the diameter of the spherical absorber using equation 2.9

$$A_a = \pi r^2 \quad \ldots\ldots 2.9$$

The radius of the spherical absorber was 0.065 m therefore the absorber area was 0.01327 m^2

The solar constant G_{sc} at the location of solar harvest was measured using solar power meter in W/m^2.

2.2.7 Determination of efficiency

Efficiency of the PDSC was calculated as the first law efficiency, η_1 which is the ratio of power output (thermal energy gained by water per second) to the power input (solar power intercepted)

Thus $$\eta_1 = \frac{\text{useful power output of device}}{\text{power input}}$$

$$\eta_1 = \frac{\dot{m}c_p\,(T_o - T_i)}{Gsc\ Aa \cos \theta i} \times 100 \qquad \text{.....2.10}$$

Where solar power intercepted by the aperture was calculated using equation 2.8,

$$\dot{Q}_s = (G_{sc})\, A_a \cos \theta_i$$

CHAPTER THREE

RESULTS AND DISCUSSION

This chapter discusses the results obtained from several experiments done on different days between 4th and 7th March 2014. The measurements were carried out to investigate the effect of the following parameters on the performance of the PDSC:

I. Performance of tracking compensated PDSC compared to non-tracking compensated PDSC
II. Performance of compensated tracking PDSC compared to non-compensated tracking PDSC

The results will therefore be discussed in the above order and not necessarily by the order in which the experiments were carried put.

3.1 Determination of concentration ratio

The concentration ratio was calculated from the geometry of the PDSC using equation 1.1

$$C = \frac{A_a}{A_r} = \frac{7.07\ m^2}{0.01327 m^2} = 532.6 \quad \ldots\ldots\ldots\ldots\ldots\ldots\ldots\ldots\ldots\ldots\ldots\ldots\ldots\ldots \quad 3.1$$

This is only a theoretical value signifying that the PDSC can increase the intensity of solar flux at the absorber by 532 times. However the actual amount of solar radiation that is reflected to the absorber is dependent of the reflectance and smoothness of the reflecting surface. The effective aperture area (A_{ae}) was calculated using equation 2.7 and the area obtained as $A_{ae} = 5.538\ m^2$. This effectively reduces C to a value of 417.3. In real practice the concentration ratio is expected to be less than 417.3 because of the effect of scratches, pits, dust, creases and polishing marks on the reflecting surface while assuming perfect dish geometry.

3.2 Performance of PDSC

3.2.1 PDSC non-tracking with thermal storage

The performance of PDSC non-tracking with thermal storage was studied with the dish at zenith. The measurements were taken on 4th March 2014. The general weather was clear and sunny most of the day and the flow rate of HTF was maintained at = 0.397g/s. The dish aperture was positioned to a point at zenith throughout the day. Table 3.1 shows the data obtained between 10.50 hrs and 17.00 hrs.

Table 3.1: Data for non-tracking PDSC with thermal storage (4th March 2014)

Time of Day Hrs	Solar Power W/m^2	T_2 °C	T_1 °C	T_o °C	ΔT °C	$\dot{Q}_s = \dot{m}c\Delta T$	$\eta = \dot{Q}_s/G_sA$
10.30	630	27.0	26.2	25.0	0.8	1.33	0.0381
11.00	920	29.3	26.0	25.2	3.3	4.49	0.0881
11.30	994	36.2	26.7	27.0	9.5	15.80	0.2870
12.00	1001	38.4	27.8	27.5	10.6	17.63	0.3180
12.30	1034	40.5	29.2	28.0	11.3	18.80	0.3280
13.00	1070	73.3	30.1	28.0	43.4	72.19	1.2200
13.30	643	72.4	31.4	29.0	41.0	68.90	1.9400
14.00	899	68.9	33.3	29.7	35.6	59.22	1.1800
14.30	1270	47.0	34.0	29.2	13.0	22.62	0.3200
15.00	1023	35.2	34.0	29.0	1.2	2.10	0.0371
15.30	825	28.5	32.3	28.9	-3.8	-6.42	-0.1400
16.00	729	27.5	30.2	28.0	-2.7	-4.49	-0.1112
16.30	800	27.0	29.0	27.0	-2.0	-3.33	-0.0751

Time of Day Hrs	Solar Power W/m^2	T_2 °C	T_1 °C	T_o °C	ΔT °C	$\dot{Q}_s = \dot{m}c\Delta T$	$\eta = \dot{Q}_s/G_sA$
17.00	726	27.0	26.3	26.4	0.7	1.16	0.0288

This data was used to plot graphs showing diurnal variation of solar power/thermal power output with the time of the day as shown in Figure 3.1.

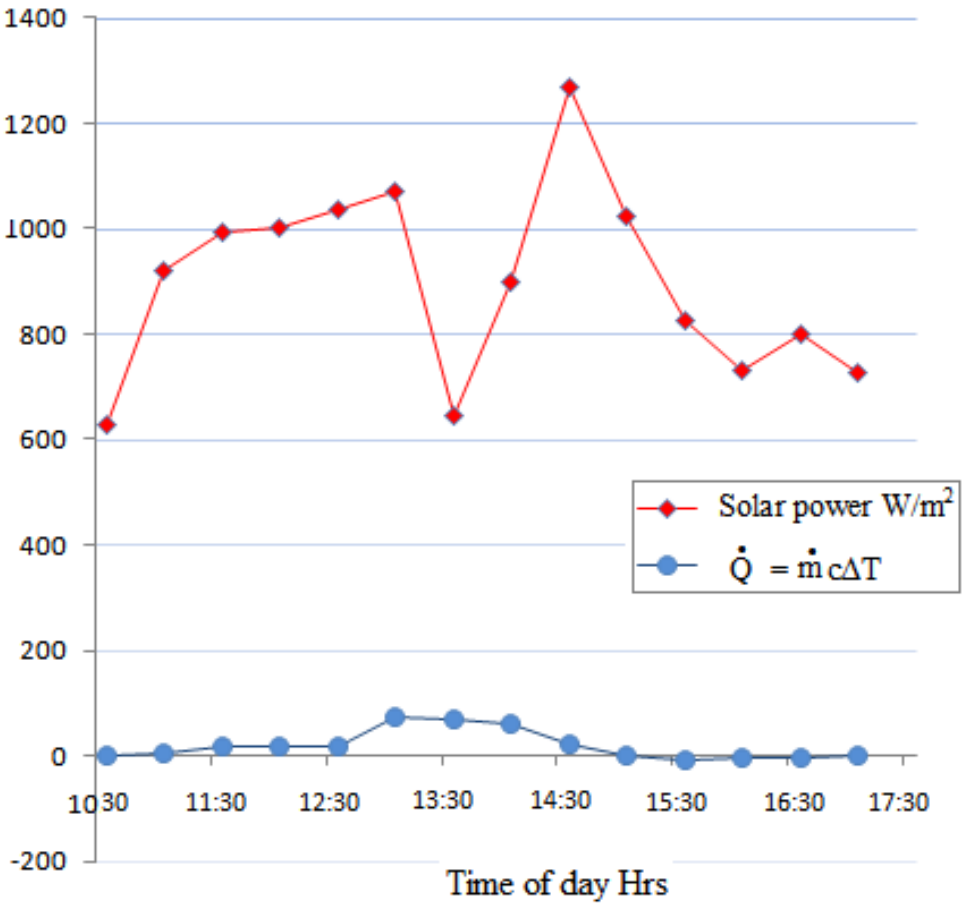

Figure 3.1: Diurnal variation of power output of non-tracking PDSC with thermal storage

Low power output was realized in the morning hours which then increased drastically to a maximum when the sun was at zenith between 13:00 hrs and 14:30 hrs as indicated in Figure 3.1. There was a sharp decrease in solar power in the period between 13:00hrs and 13:30 hrs due to cloud cover. The power output then continued to decrease in the afternoon hours when the solar beam was not perpendicular to the aperture. The power output of the SED is dependent on the intercept factor, γ which was considerably low in the early morning and late afternoon hours. The intercept factor was high when the sun was at zenith resulting to a good proportion of the perpendicular beam being reflected to the absorber. The power output decreased as the angle of incidence increased. This was so because diffuse radiation cannot be reflected to the focus, a condition that results in maximum cosine losses. Results showed negative power output between 15.30 hrs and 16.30 hrs, a situation implying that the HTF was entering the absorber region with greater thermal energy that the solar energy received by the absorber. This was true because the water inlet delivery pipe was lying on the hot ground during the experiment and as such, the amount of heat absorbed by the water before entering the SED was greater than any diffuse radiation that happened to reach the absorber. Consequently, the HTF was leaving the SED at a lower temperature than it was entering ($T_2 < T_1$), a case of negative efficiency as depicted in Figure 3.2. Appreciable power output was only confined to the interval around solar noon indicating that solar tracking was necessary for optimum working of the PDSC.

The data was also used to plot a graph showing variation of efficiency during the solar harvesting period as shown in Figure 3.2.

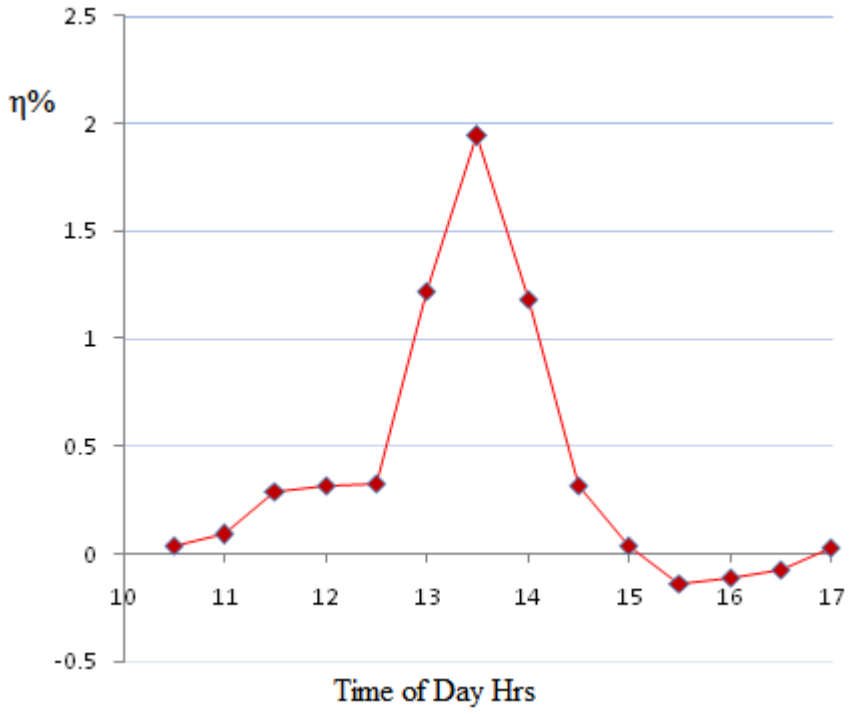

Figure 3.2: Graph of efficiency of non-tracking PDSC

Maximum efficiency (1.94%) was only achieved when the solar beam was normal to the collector and much lower efficiency at other times of the day when the solar beam was not normal to the dish aperture. This underlined the fact that solar tracking was absolutely necessary for a functional PDSC. Although the efficiency of the system was considerably low, there was evidence that the PDSC could harness solar energy for relevant use. Negative efficiency of the Solar Energy Device (SED) was indicated between 15.00 hrs and 17.00 hrs, an observation that implied HTF was transferring heat energy to the SED.

3.2.3 Performance of tracking PDSC with thermal storage

The performance of tracking PDSC with thermal storage was also studied. The measurements were taken on 7th March 2014 between 10.00 hrs and 17.00 hrs. The

general weather was clear and sunny with intermittent windy regime. The flow rate of HTF was maintained at 0.46g/s. Table 3.2 shows the data obtained.

Table 3.2: Data for tracking PDSC with thermal storage (7th March 2014)

Time of Day Hrs	Solar Power W/m^2	T_2 ^oC	T_1 ^oC	T_o ^oC	ΔT ^oC	$\dot{Q}_s = \dot{m}c\Delta T$	$\eta = \dot{Q}_s/G_sA$
10.00	187	74.0	26.3	22.0	47.7	91.94	8.87
10.30	157	74.3	26.0	23.4	48.3	93.09	10.71
11.00	155	75.6	26.3	24.5	49.3	95.02	11.06
11.30	1131	79.3	32.0	24.6	47.3	91.17	1.46
12.00	1116	98.0	30.8	25.0	67.2	129.52	2.09
12.30	1080	99.6	31.3	26.0	68.3	131.64	2.21
13.00	1159	99.6	36.2	27.7	63.4	122.20	1.90
13.30	1278	100.3	36.2	28.6	64.1	123.55	1.74
14.00	1078	99.4	35.2	31.3	63.4	122.20	2.05
14.30	1071	76.3	37.3	32.0	39.0	75.94	1.15
15.00	1061	88.0	34.5	30.2	53.5	103.12	1.74
15.30	1080	98.0	34.0	29.4	64.0	124.32	2.08
16.00	1109	79.0	34.2	29.8	44.8	86.35	1.41
16.30	925	71.3	30.0	29.0	41.3	79.60	1.55
17.00	716	65.0	29.0	27.2	36.0	69.96	1.79

This data was used to plot graphs showing variation of solar power/thermal power output of the SED with the time of the day as shown in Figure 3.3

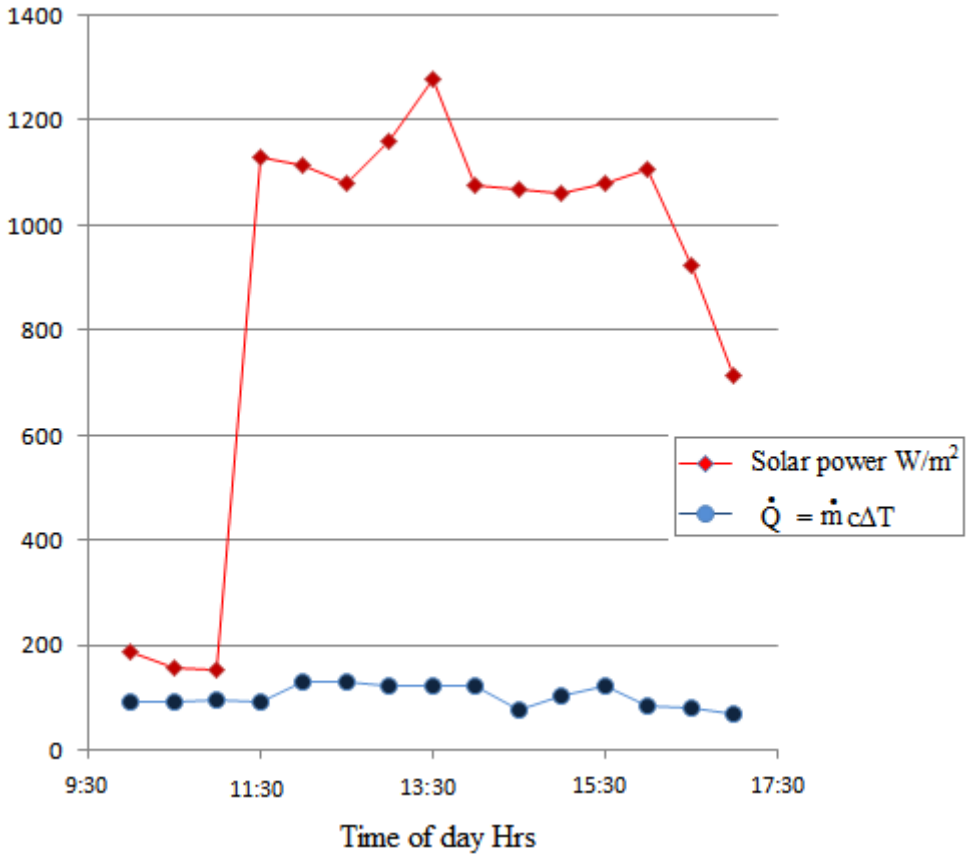

Figure 3.3: Graph of power output of tracking PDSC with thermal storage

The PDSC with solar tracking showed better performance compared to the PDSC without tracking. Figure 3.3 shows that the energy output was consistently high most time of the day and was not just confined to solar noon when the solar beam is normal to the dish. The same experiment was repeated on a different day, 6th March 2014. The general weather was sunny with cloudy intervals. The flow rate of the HTF was maintained at 0.808g/s. Table 3.3 shows data collected between 10.30 hrs and 17.00 hrs. The data obtained was used to plot graphs showing variation of solar power/thermal power output of the SED with the time of the day.

Table 3.3: Data for tracking PDSC with thermal storage (6th March 2014)

Time of Day Hrs	Solar Power W/m^2	T_2 °C	T_1 °C	T_o °C	ΔT °C	$\dot{Q}_s = \dot{m}c\Delta T$	$\eta = \dot{Q}_s/G_sA$
10.30	392	62.3	29.9	26.0	33.3	112.74	5.19
11.00	429	63.5	29.9	26.0	33.6	113.75	4.79
11.30	282	58.2	29.2	26.4	29.0	100.21	6.41
12.00	1283	56.7	30.7	27.6	26.0	90.00	1.28
12.30	1169	46.9	30.6	27.0	19.9	67.37	1.03
13.00	308	49.6	28.3	28.0	21.3	72.11	4.23
13.30	1185	92.0	31.8	29.0	60.3	204.15	3.12
14.00	1185	95.4	31.0	29.0	64.4	218.03	3.33
14.30	1187	88.5	32.2	30.3	56.3	190.60	2.90
15.00	200	65.5	28.4	30.3	37.1	125.60	11.35
15.30	187	69.8	27.6	31.0	42.2	142.87	12.05
16.00	888	66.7	27.5	29.8	39.2	132.71	2.69
16.30	792	62.4	27.4	25.3	35.0	119.17	2.72
17.00	325	54.2	26.0	25.4	28.2	95.47	5.31

This data was used to plot graphs showing variation of solar power/thermal power output of the SED with the time of the day shown in Figure 3.4.

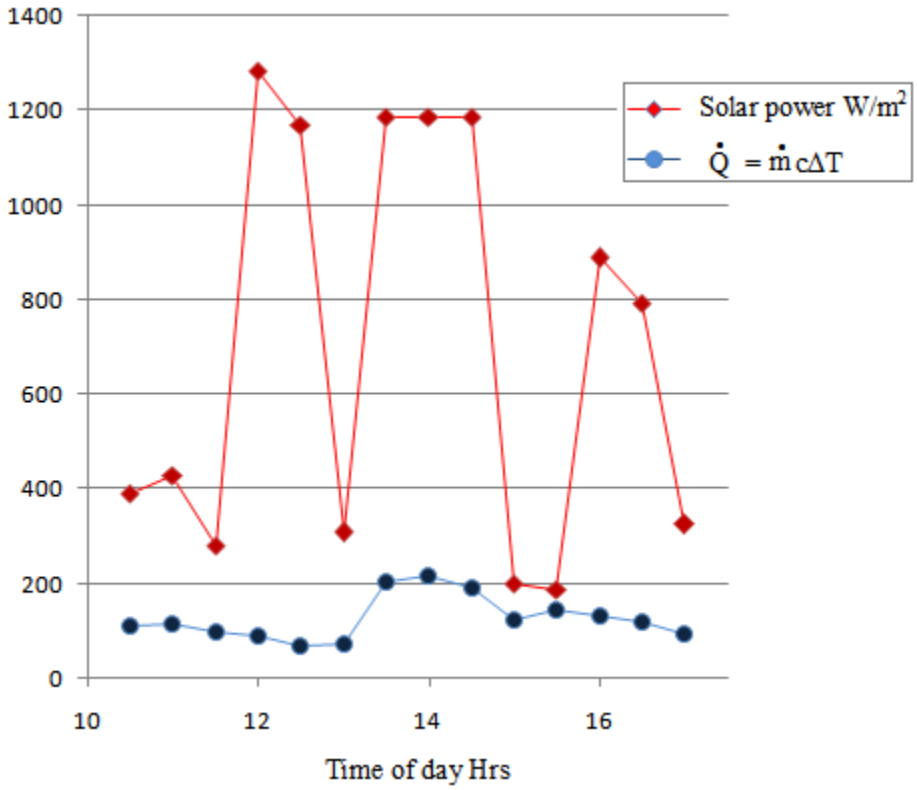

Figure 3.4: Graph of power output of tracking PDSC with thermal storage

The repeat experiment as depicted by Figure 3.4 also shows that the thermal power output is independent of solar noon orientation which is the characteristic of the non-tracking SED. Figure 3.4 shows the peak thermal output at 14.00 hrs which is 1hr past the solar noon. This meant that solar tracking was necessary for effective capture of solar energy. Maximum power output was achieved in the interval between 13.30 hrs and 14.30 hrs when the solar intensity was quite high (about 1190 W/m^2). A similar maximum output should have been expected at the period between 11.5 hrs and 13.0 hrs when solar intensity was a maximum (as high as 1283 W/m^2 during the solar noon). However this turned out to be a minimum output period possibly because of mechanical strain due to the weight of the substrate which affected the dish geometry. In the single

axial tracking, the weight of the dish and receiver had a vertical component given by equation 3.2.

$$F = mg\cos\theta \quad \ldots\ldots 3.2$$

where θ is the angle between the absorber antenna and the line of zenith.

Equation 3.2 shows that the force of deformation of the collector substrate was proportional to the value of cosθ which was maximum at 0^o when the dish aperture was at zenith. As long as the dish maintained its mechanical integrity during the solar harvesting period there was steady power output which was proportional to the solar intensity.

Comparing power output of the non-tracking and tracking devices (see Figures 3.1 and 3.3 respectively), the tracking device gave relatively steady values throughout the solar harvesting period. The non-tracking device gave low power output most part of the day except in the interval around solar noon. The efficiency of tracking PDSC with thermal storage was much higher, with a maximum of 11.06% compared to 1.94% without tracking (efficiency values in tables 3.3 and 3.2 respectively).

3.2.4 Performance of tracking PDSC without thermal storage

The relationship between power output of the tracking SED and solar power intercepted was studied in order to determine whether fluctuations in power output could be rectified by having a temporary thermal storage medium within the receiver. The measurements were done on 5th March 2014. The general weather was sunny, clear sky most of the day. The flow rate of the HTF was maintained at 0.667g/s. Table 3.4 shows the data collected between 10.50 hrs and 17.00 hrs.

Table 3.4: Data for PDS tracking without thermal storage (5th March 2014)

Time of Day	Solar Power						
Hrs	W/m^2	T_2 ^oC	T_1 ^oC	T_o ^oC	ΔT ^oC	$\dot{Q}_s = \dot{m}c\Delta T$	$\eta = \dot{Q}_s/G_sA$
10.30	889	57.7	32.0	25.0	25.7	71.82	1.46
11.00	870	63.0	33.0	26.5	30.0	83.84	1.74
11.30	1080	77.5	34.5	28.3	43.0	120.17	2.03
12.00	1176	67.0	35.2	34.0	31.8	88.88	1.36
12.30	1080	72.0	35.0	35.0	37.0	105.64	1.77
13.00	1071	73.3	34.5	31.6	38.9	108.71	1.83
13.30	1073	73.9	36.1	31.2	37.8	105.64	1.78
14.00	1061	80.0	36.7	29.2	43.3	121.01	2.06
14.30	125	77.0	35.9	27.3	41.1	114.86	16.59
15.00	1024	56.8	29.0	29.0	27.8	77.69	1.37
15.30	1023	63.4	30.8	29.0	32.6	91.11	1.60
16.00	1039	87.5	32.4	29.8	55.1	154.00	2.68
16.30	670	58.9	32.3	26.0	26.6	74.34	2.00
17.00	198	46.0	24.9	24.5	21.1	58.96	5.37

The data was used to plot graphs showing variation of solar power/thermal power output of the SED with the time of the day, Figure 3.5.

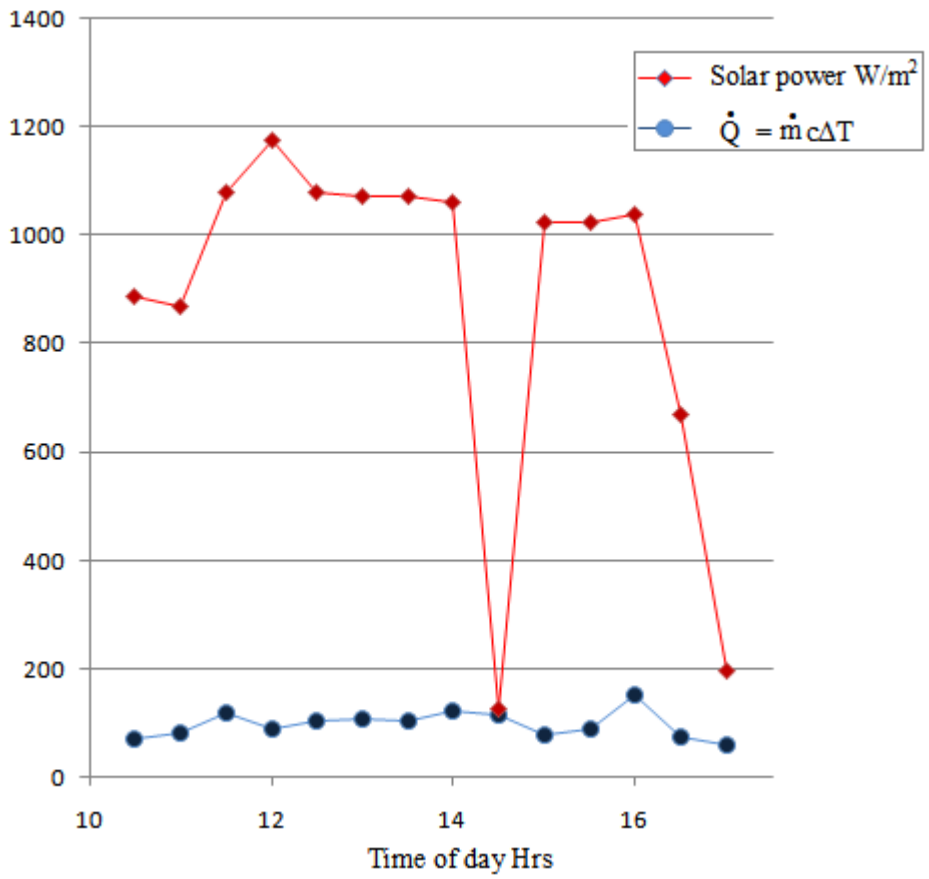

Figure 3.5: Graph of power output of tracking PDSC without thermal storage

The graph shows thermal power output directly resonating with the fluctuating solar power. However, there is observable delay in response to the solar fluctuations. The graph indicates a region of sharp decline in solar flux between 14 hrs and 15 hrs yet not accompanied by a sharp decline in the power output. This can be attributed to the heat capacity of the HTF itself and a slight contribution of heat capacity of the material encasing the HTF. The compensated device shows steadier power output even during drastic swings in the solar intensity as indicated by Figure 3.3 in contrast to fluctuating output of non-compensated device indicated by Figure3.5. These results suggest that buffering using a thermal storage media can enhance performance of the SED.

The experiment was repeated to compare the effect of energy output under shaded conditions for both thermal compensated and non-compensated PDSC.

3.2.5 Cooling curve of HTF with thermal storage

The performance of tracking PDSC with thermal storage was studied in shaded condition. A cloudy condition was simulated by disorienting the dish such that the aperture intercepted minimum solar flux. The HTF was allowed to continue flowing at the same rate as when the device was receiving intense radiation. The readings were taken at 30 s interval with the flow rate of HTF at 0.83 g/s for a period of about 8 minutes and the data tabulated as shown in Table 3.5.

Table 3.5: Cooling curve of HTF with thermal storage (5^{th} March 2014)

Time of Day	Solar Power						
Hrs	W/m^2	T_2 ^oC	T_1 ^oC	T_o ^oC	ΔT ^oC	$\dot{Q}_s = \dot{m}c\Delta T$	$\eta = \dot{Q}_s/G_sA$
0	1270	100.5	31.0	29.0	69.5	241.70	3.44
30	319	96.4	30.5	23.0	65.9	229.18	12.97
60	322	94.2	29.0	24.0	65.2	226.75	43.46
90	301	95.0	28.3	24.5	66.7	231.96	44.09
120	299	95.6	32.0	24.6	63.6	221.18	41.78
150	204	95.2	28.0	23.5	67.2	233.70	44.33
180	198	94.3	27.0	22.0	67.3	234.05	44.82
210	159	92.0	27.6	21.0	64.4	224.00	43.96
240	189	85.0	28.0	23.9	57.0	198.23	42.12
270	277	91.6	26.9	24.0	64.7	225.01	44.36
300	230	82.0	27.0	24.0	55.0	191.27	42.16
330	217	78.0	26.8	23.0	51.2	178.06	42.22
360	237	77.1	26.0	22.7	51.1	177.71	41.62
390	208	75.0	26.0	23.0	49.0	170.41	41.03

The data was then used to plot the cooling curve of the HTF shown in Figure 3.6.

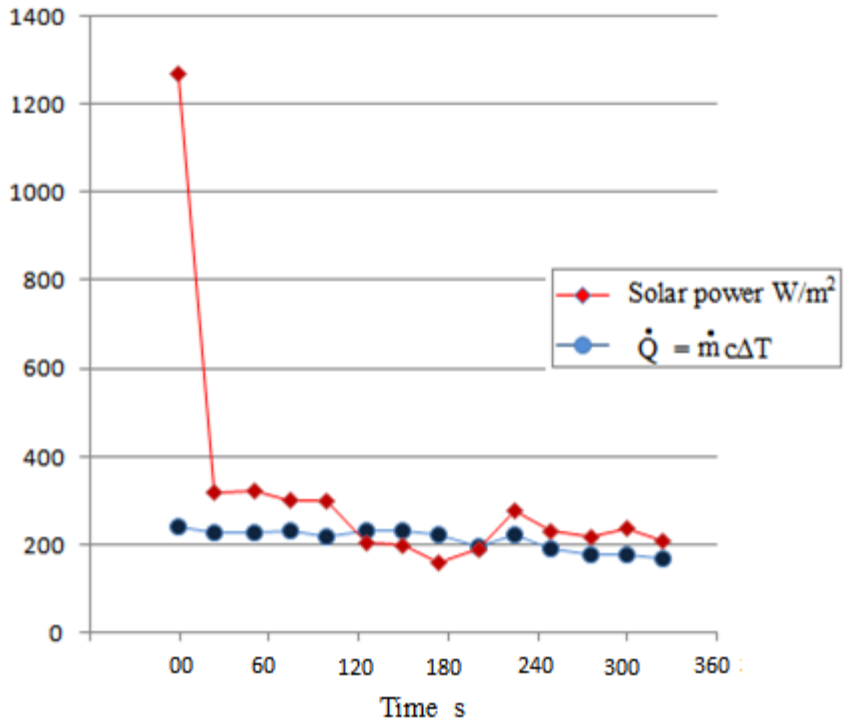

Figure 3.6: Cooling curve of HTF with thermal storage

Results show a relatively stable energy output despite the drastic solar power fluctuations. In the interval of time between 120 s and 210 s, Figure 3.6 indicates a higher power output than the solar power received. The thermal storage material compensates for the absent solar radiation by losing its sensible heat capacity. At higher temperature, it is expected that the PCM would be in molten state and the heat recovery would be the release of latent heat of fusion during freezing of the alloy. This heat is absorbed by the HTF. The latent heat of fusion is a higher density form of energy recovery than the sensible heat and thus a longer period of thermal compensation in absence of solar beam would be expected. Also since the change of state occurs at constant temperature, the PCM components serves as a temperature buffer that steadies

the power output. The maximum efficiency of the compensated device was 44.82% and minimum efficiency was 3.44% (see Table 3.5).

3.2.6 Cooling curve of HTF without thermal storage

The measurements were done on 5th March 2014 with readings taken at 30 s interval for a period of about 8 minutes with HTF flow rate of 0.667g/s. A cloudy condition was simulated by disorienting the dish aperture such as to intercept minimum solar radiation. Table 3.6 shows the data for cooling of HTF without thermal storage. The data was used to plot a graph of the cooling curve of HTF without thermal storage shown in Figure 3.7.

Table 3.6: Data for cooling of HTF without thermal storage

Time s	Solar Power W/m^2	T_2 ^oC	T_1 ^oC	T_o ^oC	ΔT ^oC	$\dot{Q}_s = \dot{m}c\Delta T$	$\eta = \dot{Q}_s/G_sA$
0	1039	75	30.8	29.2	44.2	123.52	2.05
30	324	72	31.0	29.0	41.0	114.58	6.38
60	320	71	31.0	29.8	40.0	111.79	6.31
90	325	69	31.0	27.3	38.0	106.20	6.00
120	319	78	31.0	29.0	47.0	131.35	7.44
150	189	75	31.5	29.0	43.5	121.57	11.60
180	200	72	31.8	28.9	40.2	112.35	10.14
210	218	70	32.3	26.0	37.7	105.36	8.72
240	241	68	32.0	27.6	36.0	100.61	7.54
270	392	67	32.0	28.0	35.0	97.82	4.50
300	304	66	32.0	29.3	34.0	95.02	5.64
330	312	65	31.9	28.7	33.1	92.51	5.36
360	192	64	32.0	27.9	32.0	89.71	8.44
390	230	47	32.0	28.3	15.0	41.92	3.29

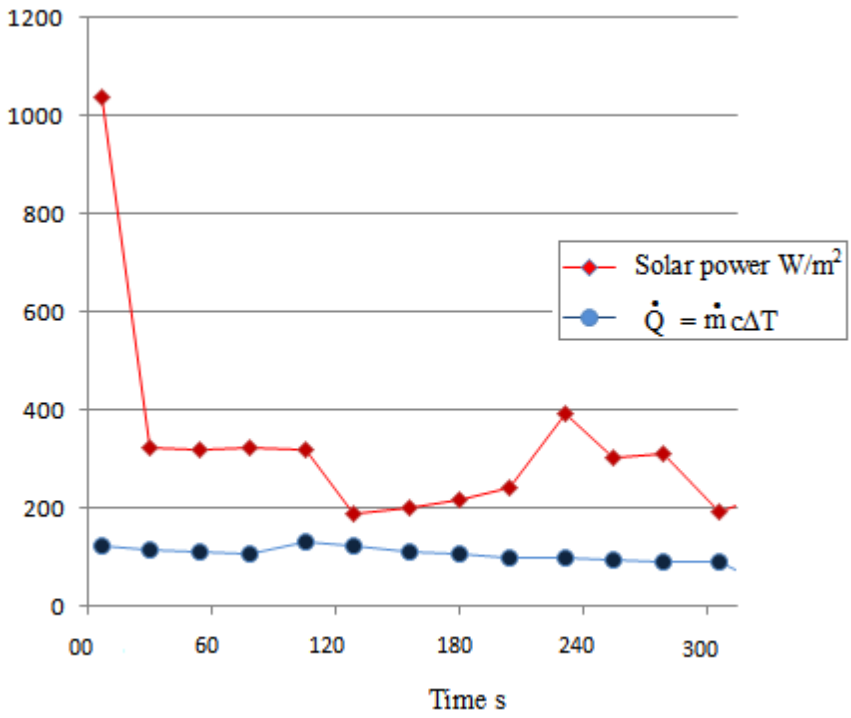

Figure 3.7: Cooling curve of HTF without thermal storage

Comparing the non-compensated and compensated devices as indicated by Figure 3.8, it can be seen that the compensated device gives steadier energy output than the non-compensated device. The region of compensation in the Figure 3.8 (b) indicates a situation where the device gives a greater energy output than the solar energy intercepted. This proves that there is energy recovery from the PCM storage.

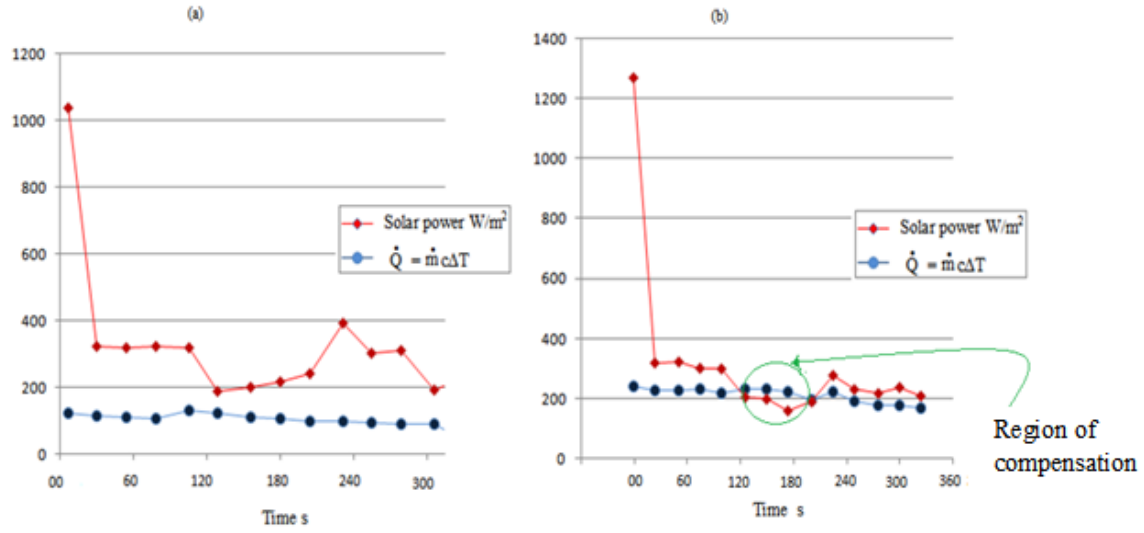

Figure 3.8: Comparison of cooling of HTF: (a) without thermal storage (b) with thermal storage

The maximum efficiency was 11.6% and the minimum efficiency was 2.05% (Table 3.6). Analysis shows a higher efficiency when there is thermal storage in the absorber. The thermal storage component therefore improved the performance of solar energy collector. The graph of cooling with thermal storage in the time interval between 120 s and 210 s shows higher energy output than the solar energy received. This was due to the energy recovery from heat capacity and latent heat effects of the PCM.

CHAPTER FOUR

CONCLUSIONS AND RECOMMENDATIONS

4.1 Conclusions

A parabolic dish solar collector with a concentration ratio of 532.6 was fabricated and tested. The performance of PDSC was studied under different solar harvesting conditions it was clear that best results were obtained when the device was sun tracking and having the thermal storage component. However, this was not without challenge as the system was a single axis tracking device which did not cater for diurnal and seasonal variation of solar declination angle. For this reason a certain proportion of radiation could not reach the absorber leading to lower efficiency than expected. The temporary thermal storage medium which was SnPb alloy at the absorber was found to enhance performance of the PDSC by stabilizing the power output.

4.2 Recommendations

- To maximize on the intercept factor, a dual axis tracking system should be studied so as to continuously focus the solar flux at the receiver accurately.
- The mechanical solar tracker was an approximation of tracing the position of the sun across the sky dome. This could not give a perfect perpendicular solar flux intercept, resulting in deviations of the beam from the focus. It is recommended that a microprocessor-based control unit be mounted on the concentrator to provide precise tracking.
- The position of the receiver in the prototype design was outside the dish aperture and thus exposing the receiver to regimes of wind and droughts interfering with the desired heat exchange of the HTF. It is recommended that the dish geometry be redesigned to have the absorber position well shielded from prevailing wind and droughts. The ambient temperature around the receiver can be stabilized by enclosing the dish with a light transparent membrane to act as heat trap. The

amount of heat conserved by the heat trap could surpass the fraction of solar flux reflected by the heat trap membrane.

- A more accurate data collection method could be used by employing a data logger with appropriate thermometer probes and software to monitor the performance of the PDSC.
- If the system is intended for large scale steam generation for electricity, then it can be hybridized with photovoltaic solar panel and buffering achieved by use of DC accumulators and the energy recovery process done via an inverter.
- It is also recommended that further study be done on other materials and alloys which have phase change properties at lower temperatures.

REFERENCES

Abhat, A. (1983). Low temperature latent heat thermal energy storage: heat storage materials. *Solar Energy, 30*(4), 313–331.

Ari, R. (1985). *Active Solar Collectors and their Applications*. New York: Oxford University Press.

Banaszek, J., Domanaski, R., Rebow, M. & El-Sagier, F. (1999). Experimental study of solid – liquid phase change in a spiral thermal energy storage unit. *Applied Thermal Engineering, 19,* 1253–1277.

Beggs,C., (2009). *Energy: Management supply and conservation*. Oxford, UK. Elsevier publishers.

Bill, B.P. (1980). *Proceedings of a Regional Seminar and Workshop on Utilization of Solar Energy in Hot Humid Urban Development, held at Singapore,* 30th Oct – 1st Nov, 1980

Buddhi, D. & Sawhney, R. L. (1994). Proceeding of thermal energy storage and energy conversion. School of energy and environmental studies. Devi Ahilya University. Indore, India. February 24–25.

Cengel, Y. A. (2003). *Heat and Mass Transfer: A Practical Approach*. New York, USA: McGrow-Hill.

Christopher, L., Martin, D. & Yogi, G. (2005). *Solar energy pocket reference*. Earthscan

Classroom energy (2014). Retrieved from: http://www.classroom-energy.org/energy_09/3.html

Duffie, J. A. (1991). *Solar Engineering of Thermal Processes*. 2nd Edition USA: A Wiley Interscience Publishers

Energy (2000). "*World Bank Energy Report*," Retrieved from http:// www. undp. Org/seed/eap/publications /1999/19.99 a.

Energy Technology Systems Analysis Program, (2013), Thermal Energy Storage. International Renewable Energy Agency (IRENA). Technology brief EIT.

Farid, M. M., Khudhair, A. & Razacksak, A. S. (2004). A review of phase change energy storage: materials and applications. *Energy Conversion and Management 45*, 1597–1615.

Fernanda, G. P. (1988). Salt hydrates used for latent heat storage: corrosion metals and reliability of thermal performance. *Solar Energy 41*(2) 193–197.

Garg, H.P., Mullick, S. C. & Bhargava, A. K. (1985). *Solar Thermal Energy Storage.* Dordrecht, Holland: D. Reidel Publishing Co.

Geyer, M. A. (1991). Thermal Storage for Solar Power Plants, Ch. 6 of C.-J. Winter, R.L. Sizmann, L. L. Vant-Hull (Eds.), .Solar Power Plants., New York: Springer-Verlag,

Gilbert, M. (2004). *Renewable and Eficient Electric Power Systems,* New Jersey: John Wiley & Sons, In. Hoboken.

Gillet, W. B. (1985). *Solar Collectors*. Dordecht: Dreidel publishing company.

Global Economic Symposium (2014) The Energy Crisis and Climate Change. Retrieved from http://www.conserve-energy-future.com/causes-and-solutions-to-the-global-energy-crisis.php.

Gustafsson, M., Bo, H. & Seterwall. F. (1998). Paraffin waxes and their mixture as phase change materials (PCMs) for cool storage in district cooling system. IEA Annex 10, 45–56, Adana, Turkey. April 16–17.

Hale, D.V., Hoover, M.J. & O'Neill, M.J. (1971). Phase Change Materials Hand Book, Report no.HREC- 5183-2LMSC-HREC D225138. NASA. Marshal Space Flight Center. Alabama.

Harvey, L. D. (2010). *Carbon-Free Energy supply*. Washington, USA: Earthscan publishers.

John, W., Twidel, D.S. & Weir, A.D. (1986). *Renewable Energy Resources*, London: ELBSLE and F.N Spon Ltd.

Kawira, M. (2011). *Fabrication and Characterization of a Prototype Parabolic Trough Solar Concentrator for Steam Production*. MSc Thesis, Jomo Kenyatta University of Agriculture and Technology, Nairobi, Kenya.

Kelly, B. D. & Lessley, R. L. (1994) Investigation of Commercial Receiver Thermal Storage and Steam Generator Issues, ASME Int. Solar Energy Conf. San Francisco (United States)

Lane, G. A. (1983). Solar Heat Storage: Latent Heat Materials, Vol. I. Florida, USA: Boca Raton.

Marion, W. & Wilcox, S. (1994). *Solar Radiation Data Manual for Flat-Plate and Concentrating Collectors*. NREL/TP- 463-5607. Golden, CO: National Renewable Energy Laboratory, 252 p.

Medved, S., Meglic, B. & Novak (2009) "Solar cooker designs" Retrieved from http://solarcooking.wikia.com/wiki/File

Mridul, K. (2006). "Parabolic Dish Solar Concentrator" Retrieved from http://sunenergyworld.blogspot.com

National Energy Policy (May 2004), Sessional Paper No. 4 on Energy. Retrieved from: http://www.renewableenergy.go.ke/downloads/policy-docs/sessional_paper_4_on_energy_2004.pdf

Orel, Z. C., Gunde, M. K. & Hutchins, M. G. (2002) Spectrally selective solar absorbers in different non-black colours. Proceedings of WREC VII, Cologne on CD-ROM.

Price, H., Lufert, E. & Kearney, D. (2010). *Advances in Parabolic Trough Solar Technology*. Sol Energy-T ASME, London.

Rai, G. D. (1987). *Solar Energy Utilization*. (3rd Ed.). New Delhi, India: Khanna Publishers.

Saperstein, A. M. (1975). *Physics: Energy in the Environment*. Canada: Little Brown and Company.

Sayigh, A. A. M. (1979). *Solar Energy Applications in Buildings*. New York, USA: Academic Press.

Sharma, S. D. (1999). *Study of thermal energy storage in phase change materials for low temperature solar applications*. Ph.D. Dissertation, Devi Ahilya University, Indore, India.

Solar and Wind Energy Resource (SWERA, 2010). "*Renewable Energies in Africa*", Retrieved from http:// www.swera.unep.net

Stefan, G., Kenneth, M. & Kim, P. (2006). Equal opportunity for biomass in greenhouse gas accounting of CO_2 capture and storage: a step towards more cost-effective climate

change mitigation regimes. *Mitigation and Adaptation Strategies for Global Change*, 11:1083–1096.

Thomas, B. J. & Goldenberg, J. (1993). *Energy for Sustainable World*. New York: John Wiley & Sons.

Thulasi, T.C., Karmakar, S. & Rao, D.P. (1994). Solar box cooker: part 1 modeling. *Solar Energy* 52(3), 265–272.

Tiwari, G.N., Rai, S. N., & Santram, S. M. (1988). Performance prediction of PCCM collection cum-storage water heater: quasi-steady state solution. *Energy Conversion and Management,* 28(3), 219–223.

Wackelgard, E., Niklasson, G. A. & Granqvist, C.G. (2001). *Selective Solar Absorbing Coatings.* In: Gordon J, editor. Solar energy: the state of the art. Germany: ISES; p. 109–44.

Zalba, B., Marin, J. M., Cabeza, L.F. & Mehling, H. (2003). *Review on thermal energy storage with phase change: materials, heat transfer analysis and applications. Applied Thermal Engineering 23*, 251-283.

APPENDIX

This section consists of photographs taken during the experiment.

Plate A1: The Solar power meter during the experiment.

Plate A2: Mechanical solar tracker

Plate A3: Flow Rate meter and thermocouple thermometer used in the experiments

Plate A4: Thermocouple thermometer during the experiment.

Plate A5: Construction of parabolic dish at engineering workshop JKUAT.

Plate A6: Experiment in session.

Plate A7: Small scale heating application of PDSC
[National Science Foundation 2008]